

A detailed review of perovskite solar cells: Introduction, working principle, modelling, fabrication techniques, future challenges



Sagar Bhattacharai^{a,*}, Asya Mhamdi^b, Ismail Hossain^c, Yassine Raoui^d,
Rahul Pandey^{e,**}, Jaya Madan^{e,***}, Abdelaziz Bouazizi^b, Madhusudan Maiti^f,
Dipankar Gogoi^g, Arvind Sharma^g

^a Department of Physics, Arunachal University of Studies, Namsai, 792103, Arunachal Pradesh, India

^b Laboratory of Condensed Matter and Nanosciences, Group of Organic Electronic and Molecular Photovoltaics Devices, Faculty of Sciences of Monastir, University of Monastir, 5019, Monastir, Tunisia

^c School of Natural Sciences and Mathematics, Ural Federal University, Yekaterinburg, 620000, Russia

^d CHOSE (Centre for Hybrid and Organic Solar Energy), Department of Electronic Engineering, University of Rome "Tor Vergata", 00133, Rome, Italy

^e VLSI Centre of Excellence, Chitkara University Institute of Engineering and Technology, Chitkara University, Rajpura, Punjab, 140401, India

^f C. V. Raman Global University, Department of Electronics and Communication Engineering, Bhubaneswar, Odisha, 752054, India

^g Department of Basic and Applied Science, National Institute of Technology, Jote, 791113, Arunachal Pradesh, India

ARTICLE INFO

Keywords:

Review
Perovskite
Perovskite solar cells
Photovoltaic
Transport layers
Simulations
SCAPS-1D

ABSTRACT

Researchers worldwide have been interested in perovskite solar cells (PSCs) due to their exceptional photovoltaic (PV) performance. The PSCs are the next generation of the PV market as they can produce power with performance that is on par with the best silicon solar cells while costing less than silicon solar cells. The efficiency of PSCs has increased from 3.81% to 25.7% within a decade, demonstrating their immense potential. In this review, the advantages of PSCs and the evolution of efficiency with various configuration are summarized and discussed. The manufacture of PSCs on a large scale and the fabrication of perovskite films are described as well. Despite their advantages, PSCs have encountered numerous problems, including toxicity and degradation in the presence of moisture, oxygen, and UV light. Thus, we emphasize this line added to the difficulties preventing the commercialization of PSCs, as well as the road map towards commercialization are thoroughly examined.

1. Introduction

Since the previous decade, advances in photovoltaic technology have transformed the field of study in quest of a superior replacement for currently used energy sources. Owing to the superior results, the research community is expanding in relation to these energy sources. As the Earth receives a tremendous amount of solar radiation that is renewable and environmentally friendly in nature.

* Corresponding author.

** Corresponding author.

*** Corresponding author.

E-mail addresses: sagarbhattacharai012@gmail.com (S. Bhattacharai), rahul.pandey@chitkara.edu.in (R. Pandey), jaya.madan@chitkara.edu.in (J. Madan).

It can be used for the direct electricity production with the help of Photovoltaic (PV) devices. These devices convert solar radiation directly into electricity by employing semiconductor devices known as solar cells. The most abundant renewable energy source in the universe is solar energy, yet its potential has not been exploited efficiently or the solar cells in the market. The affordability of solar energy can be enhanced either by increasing the efficiency of a solar cell or by reducing its manufacturing cost. Especially silicon is most widely used semiconductor material found in today's most commercialized solar-powered gadgets. But production cost is at the higher side for silicon-based PV devices compared to other thin film technologies [1].

Moreover, Si-based solar cell technologies are hampered by the fact that Si solar cell lose efficiency more quickly as the temperature rises [2]. The high-energy need for silicon production and expensive installation cost are the main weaknesses for efficient and large-scale production of the Si-based Solar cell. Since 2009, a considerable focus has been on the usage of perovskite semiconductor material in contemporary solar systems to tackle these issues associated with the solar cell material, several attempts have been made to obtain more excellent power conversion efficiency (PCE) at the least manufacturing cost [3–6]. The intrinsic qualities of perovskite-based solar cells, such as higher optical absorption properties, higher carrier mobility and longer carrier diffusion length, led to significant improvement in conversion efficiency and grabbed the interest of researchers [7]. Kojima et al. were the ones to first launch the expedition to the perovskite solar cell in 2009, reporting a PCE of 3.81% and 3.13% using iodine (I) and bromine (Br) as halide materials, respectively [8]. It is also fascinating to note that in less than ten years, the light-absorbing material of MAPbI_3 was utilized in 2019, which significantly enhanced efficiency of up to 22.1% [9]. Parallel to this, a number of earlier research claimed that structural modifications to perovskite solar materials could result in comparable results and a significantly increased efficiency. Alternative studies have shown that other materials, such as Ge and Sn, can be used to substitute the lead in the perovskite materials. To improve device outputs, the methyl-ammonium element can potentially be switched out for equivalent materials such as formamidinium (FA) and Cesium (Cs). The most recent studies by Bhattacharai et al., Abdelaziz et al., Raoui et al. also demonstrated the successful fabrication of a PSC device that is significantly more efficient [10–12]. For the various device modelling of the perovskite solar cells, unique perovskite layers with narrower bandgaps, e.g., CsSnI_3 (1.3eV) and FASnI_3 (1.41eV), can also be offered [13,14]. For the perovskite solar cells' future performance, Cesium (Cs) can be substituted for Methyl-ammonium (MA) with great efficiency.

It can also be mentioned that the new manufacturing techniques of altering the much superior active layer allowed scientists to simultaneously achieve more efficient and cost-effective solar cells [15]. The graded active layer has different bandgaps that absorb a broader range of photons incident on the device. Also, the graded perovskite active layer (PAL) can enhance the device's stability and increase the photon generation rate. Secondly, in graded PSCs, the combination of two layers further assists in extracting the smaller wavelength photons. Moreover, together, they improve the efficiency of PSC than the conventional single-layered PSC. It can be noted that the carrier transport materials (CTLs) play a substantial role in the swift flow of the carriers within the PSC device. So, optimizing the CTLs in term of optoelectronic proprieties and energy level alignments improves the transport of free charges carrier (electrons and holes) and decreases recombination during carrier transportation for efficient extraction at the electrodes [16].

The presence of CTL helps in getting higher conversion efficiencies; however associated interface defects increases the interfacial recombination within the device [17]. Therefore, a CTL free approach can be adopted, this will possibly solve the problem regarding the recombination losses and device fabrication for its simplicity [18]. Secondly, the CTL-free approach can also reduce the hysteresis as well [19]. However, removing CTL also results in poor stability; therefore it is important to tackle stability-related issues beforehand by material or device engineering before adopting CTL free approach. A monolayer PAL with a CTL-less approach can be suggested to sort out the abovementioned problems. The uniform alternative of the toxic Pb material improves the device's lifetime and eco-friendly solar cell manufacturing [20]. The perovskite active layer offers a higher absorption coefficient, which is suitable for device outputs [21]. Although the substantial progress in the materials and device structures resulted in greater efficiency and a longer lifespan of PSCs, we do not fully understand the detailed mechanisms behind these improvements.

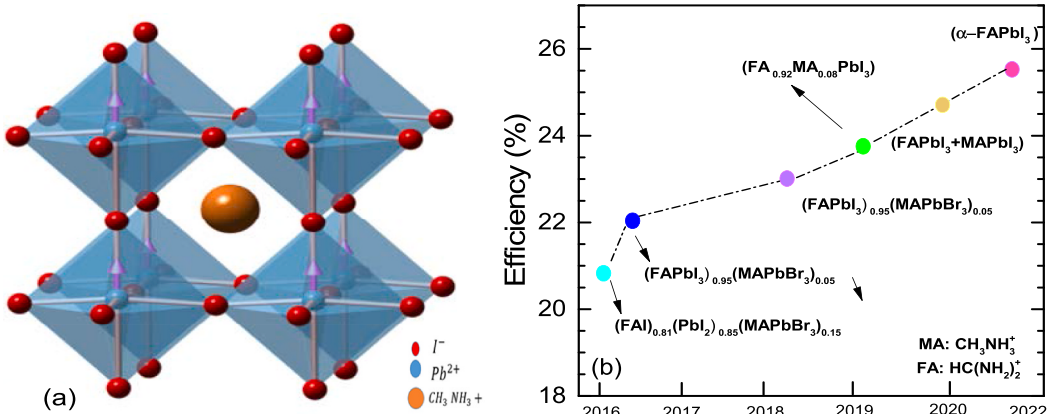


Fig. 1. (a) The crystal structure of a perovskite, and (b) The roadmap with the highest efficiencies of different perovskite solar cell technology certified by the NREL, 2019.

2. Perovskite solar cell structures

2.1. ABX_3 chemical structure

The calcium titanate (CaTiO_3) molecule's structural makeup is comparable to that of the perovskite substance [22], it has an ABX_3 chemical structure. Perovskite materials' layered structures with an octahedral cubic lattice have recently attracted a lot of attention due to its intrinsic properties. In the composition, the group A (methylammonium, CH_3NH_3^+ /MA⁺, or formamidinium, $\text{CH}(\text{NH}_2)_2^+$ /FA⁺) occupies the vertex of the face-centred cubic lattice, while metal cation B (Pb^{2+} , Sn^{2+} , etc.) and halogen anions X⁻ (Cl⁻, Br⁻, or I⁻, or coexistence of multiple halogens) occupy the centre and apex of the substance [23]. The metal-halogen octahedral are connected to produce a stable three-dimensional network structure. The crystal structure is depicted in Fig. 1 (a) [24]. Moreover, different perovskite solar cell efficiency is reported in Fig. 1 (b), along with their best efficiencies till date is mentioned [25]. (NREL, 2019).

The tolerance factor, as illustrated below, limits the size of three ions and the stability of the perovskite structure [26].

$$t = \frac{R_B + R_X}{\sqrt{2}(R_A + R_X)}$$

The ionic radii of the A, B, and X site elements are R_A , R_B , and R_X , respectively. The empirical ionic radii can be calculated using the formula at ambient temperature. For t-values near 1, the perfect cubic perovskite structure exists in a few circumstances. However, further perovskite structural aberrations typically develop ($0.75 < t < 1$). The specifics of these aberrations significantly impact the physical characteristics of perovskites. Especially the electronic, magnetic, and dielectric properties are critical for many perovskite applications. The organo-metallic halide perovskite family, which differs from the alkali metal halide perovskite family, was discovered more recently but it has generated interest because of its favourable optoelectronic characteristics and possible applications in low-temperature device constructions. The photo- and ionic conductivity and semiconducting characteristics of organometallic halide perovskite have piqued the attention of organic light-emitting diodes (OLEDs) and thin-film transistor applications as well. CsPbCl_3 and CsPbBr_3 were the first halide perovskite compounds reported in 1893 [27]. Protesescu et al. recently observed that nanocrystals of CsPbX_3 perovskite emitted brilliant light with a broad colour spectrum while CsPbX_3 , CsSnX_3 (X = Cl, Br, and I) was the discovered in 1920 [28]. It is also need to be mentioned that at low temperatures (12 °C), CsSbBr_3 exhibited a deformed tetragonal structure, whereas CsSnI_3 has an orthorhombic structure.

It was discovered that the $\text{CH}_3\text{NH}_3\text{SnBr}_x\text{I}_{3-x}$ (x = 0–3) has a cubic structure, with unit cell parameters of $a = 6.24 \text{ \AA}$ (x = 0), $a = 6.01 \text{ \AA}$ (x = 2), and $a = 5.89 \text{ \AA}$ (x = 3). Where a is the dimension along the edge of a unit cell on the x-axis. The discovered perovskites is of bright in colour and having a good conductivity. Soon after, Jiang et al. proposed organic Pb-based tri-halide perovskites, which has shown tremendous success in solar cell applications [29]. The structure information of $\text{CH}_3\text{NH}_3\text{PbX}_3$ (X = Cl, Br, and I) was examined in details, with the unit cell parameters; $a = 5.68 \text{ \AA}$ (X = Cl), $a = 5.92 \text{ \AA}$ (X = Br), and $a = 6.27 \text{ \AA}$ (X = I), respectively. According to a recent study, halide perovskites (ABX_3) shows a promising material for the futuristic applications in photovoltaics [30].

2.2. The carrier transport materials

The perovskite solar cell devices are made of an active layer stacked between ultrathin carrier transport materials, such as a hole transport layer (HTL) and an electron transport layer (ETL). The band alignment depends on their energy level, electron affinity, and ionization potential. The ultra-thin layers with low electron affinities and ionization potential serve as hole-transporting materials, while higher electron affinity and ionization potential acts as electron-transporting materials [31,32]. Consequently, a more thorough

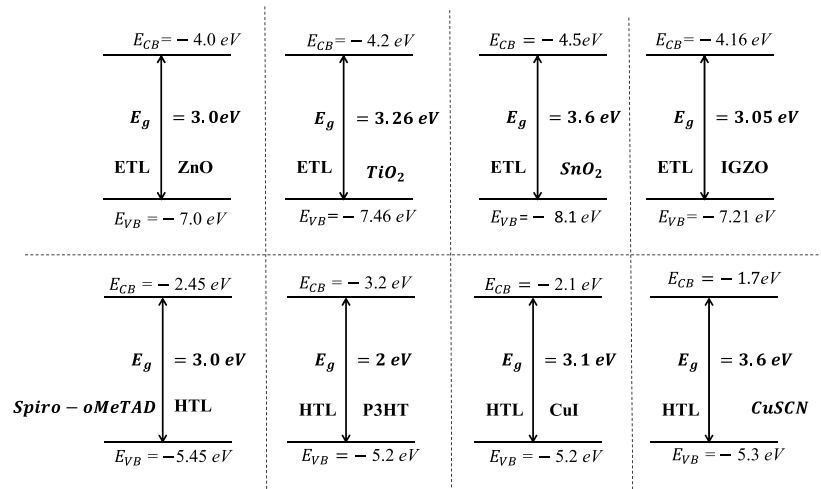


Fig. 2. Energy level diagram of different layers with HTL, ETLs.

explanation of layers is provided below.

Hole transport layer: Electron-blocking materials are used as hole transportation materials in PSCs. The hole transport layer (HTL) assists in injecting the hole from the perovskite active layer and transfers the injected hole to the back electrode. The hole-transport layer also works as an electron-blocking layer that prevents electron flow [33–36]. The typical hole transport layers are, Spiro-OMeTAD (2,20,7,70-tetrakis-(*N,N*-di-p-methoxyphenylamine)-9,90-spiro-biuroene), P3HT (Poly(3-hexylthiophene –2,5-diyl)), CuI (Copper(I) iodide), CuSCN (Copper(I) thiocyanate), etc.

Electron transport layer: The layer that assists the injected electrons from the perovskite active layer to the front electrode is ETLs in the PSCs. The electron-transport layer also works as a hole-blocking layer that prevents the release of the holes to the front electrode, respectively [33,37–39]. The typical electron transport layer is ZnO (Zinc Oxide), TiO₂ (Titanium Dioxide), SnO₂ (Tin (IV) oxide), IGZO (Indium-gallium-zinc oxide), PCBM (6,6-phenyl-C₆₁-butyric acid methyl ester), etc.

As far as the Carrier transport layers energy level details, the detailed description of energy levels of various carrier transport layers is shown in Fig. 2 [40,41] (both electron and hole transport layers, ETL and HTL). Choosing the electron transport layer such as ZnO, TiO₂, SnO₂, and IGZO provides superior electron flow to the electrodes. While the hole transport layer Spiro-OMeTAD, P3HT, CuI, and CuSCN provide the swift flow of holes to the back electrode, respectively.

The details of the Electrodes utilized in the solar cell device structure are shown below.

Anode: The anode in a solar cell structure plays a vital role in collection of generation of the carriers. Because of its low reflectivity, and high transmittivity with good electrical conductivity, high work function, and ease of patterning, fluorine doped tin oxide (FTO) is employed as the top electrode, which serves as an anode (the anode removes electrons (adds the electrons to the “holes”) when a current passes through the device) [42,43].

Cathode: Like the anodes, the cathode also substantially collects the generated holes from the absorption layer. When a current flows through the device, the cathode (which may or may not be transparent depending on the PSC kinds) receives holes. There are few most stable and low work functions cathodes, such as aluminum (Al) and silver (Ag), Gold (Au), Platinum (Pt) that are often employed as cathodes [44,45].

The detailed value of the different anodes and cathode with their values of the work functions has been provided below in Fig. 3.

The working principle of Perovskite Solar Cell is shown below in details.

In a PV array, the solar cell is regarded as the key component [46]. Semiconductor materials are used to design the solar cells, which use the PV effect to transform solar energy into electrical energy [46,47]. To perform its duty satisfactorily, it needs to have the maximum PCE feasible [45]. To design highly performant SCs and comprehend PV action, it is vital to comprehend the fundamental processes or steps that are carried out in the SC layers and the purpose of each component [48]. A portion of the photons with energy greater than Eg that strike solar cells are absorbed by the semiconductor layer.

According to Fig. 4, holes and electrons (electrons in the conduction band and holes in the valence band, respectively) are transported in various directions by photons that have enough excitation energy ($E > E_g$) to be absorbed [46]. Due to the difference in the binding energies of excitons, in perovskites, excitons can interact to form new excitons or generate (free holes and electrons) free carriers to generate current [8]. The e-h pairs are generated in the field region, and under the influence of this field, they are then separated. As a result, holes go to the p-side and electrons to the n-side. At the N-side and P-side field area boundaries, certain electrons and holes build up and eventually neutralize some of them. The remaining electrons and holes travel to the load via the outside circuit [45]. HTL gathers the free holes and electrons, ETL, followed by the metal electrode and FTO [8]. The electrostatic field not only causes

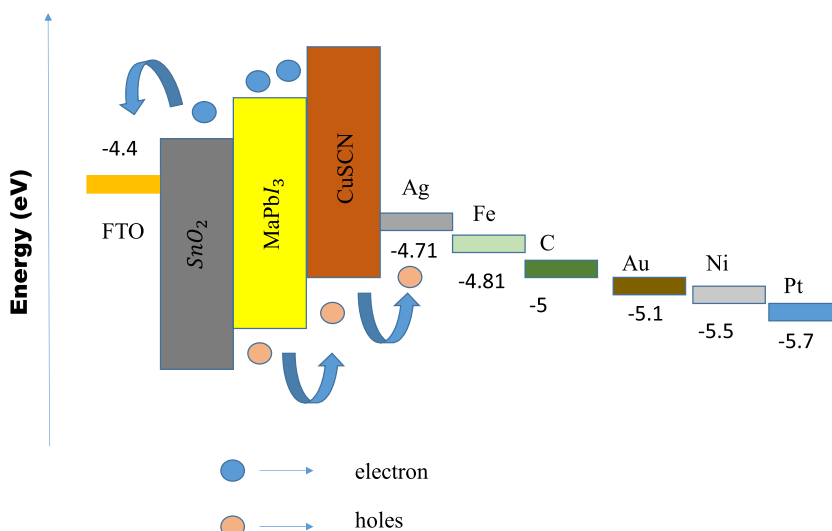


Fig. 3. The different anodes and cathodes with their values of the work functions. Metals with different work function helps in tuning the magnitude and direction of electric field for better movement of light generated charge carriers. Therefore, number of electrodes has been brought forward in this figure.

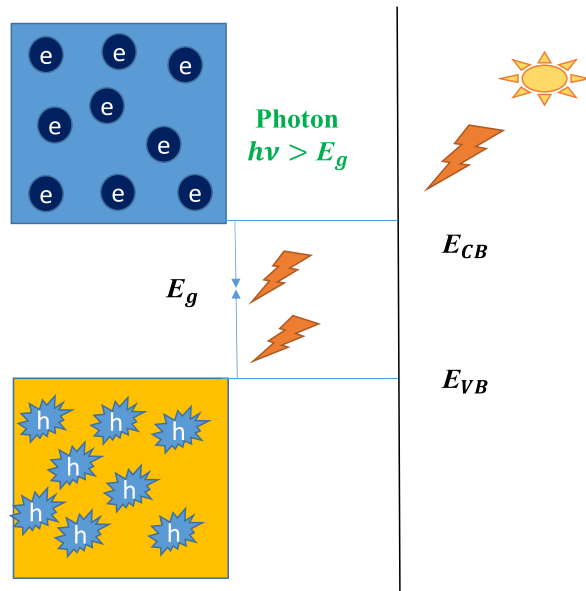


Fig. 4. Carriers generation (electron-hole pair) in a semiconductor [49].

the P-region to have positive electricity and the N-region to have negative electricity, but it can also partially offset the effects of the potential energy barrier.

The absorbed photons can cause the transition of electrons and holes with sufficient excitation energy ($E > E_g$). The bandgap of the absorbing layer of the solar cell can be obtained as shown below,

$$E_g = E_c - E_v \quad (1)$$

The generated electrons flow in the conduction band while the holes in the valence band travel in opposite directions. Without recombination, the carriers produced around the p-n junction reach the space charge area. Near the p-n junction, excess electrons and holes form an electric field that runs in the opposite direction as the potential energy barrier, as expressed in Fig. 5. Internal electric fields cause holes to diffuse into the p-type area and electrons to flow into the n-type region. As a result, there are too many holes in the p-type area, and the electrons in the n-type region are in the same boat.

The present scenario is to obtain a highly efficient PSC device with better device output parameters, including external quantum efficiency. However, the literature review reveals that lesser outputs due to improper selection of the perovskite materials, low power conversion efficiency, the toxicity of Pb in active layers, and shorter lifetime are prohibiting factors that considerably degrade the device performances. Hence, to overcome such as efficiency problem has been solved in distinct ways. Primarily, the device's efficiency should be increased by improving suitable perovskite materials and the proper selection of the carrier transport materials (ETLs and HTLs). Tertiary, using the graded perovskite materials to obtain much better efficiency, Fourthly, the toxic free perovskite active

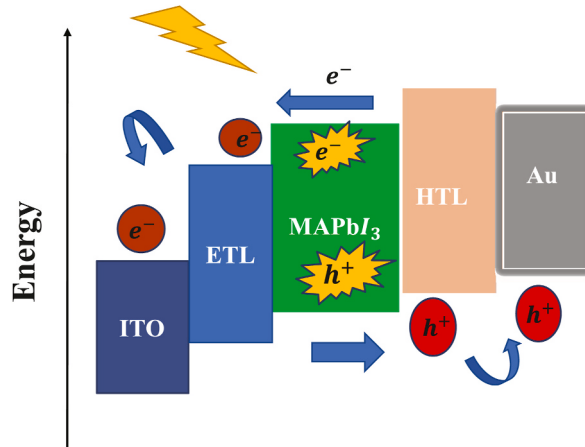


Fig. 5. The schematic solar cell diagram displays the generation of excitons and carrier transport states formed by photon absorption.

layer with better optoelectronic property. Fifthly, the more stable active layer that can be found by replacing Sn or Ge in perovskite materials respectively. Therefore, before the potential of this technology is fully realized, many obstacles must be overcome [46]. These comprise:

Photon absorption- Excitons generation rate: Most light fractions can't reach the perovskite material for the carrier transport layer in the PSC. Hence, the CTL-free approach can benefit the total extraction of photons and the generation of excitons to propose a high-performing device architecture. The small generation of the carriers in the active layer can be one of the most problematic issues in the PSC devices [47].

High carrier recombination: The carrier recombination is a major one that degrades the device efficiency due to electron and hole recombination in the perovskite materials. Due to this, it cannot take part in excessive extraction in the electrodes. The thin perovskite active layer materials cannot generate the higher photon, resulting in a smaller current density in the PSC devices [48]. While the thicker perovskite material impacts in high recombination rate, which impacts the overall performance of the PSC. Hence, to overcome such losses in devices, optimizing the thickness of the perovskite materials with a defect-free approach can be proposed. The double CTLs also assist in the smooth transport of electrons and holes.

Lesser efficiency: The less efficiency in most perovskite solar cells is a prime concern for device-related fabrication. The comprehensive bandgap materials often offer lesser efficiency due to minor electrical outputs such as current density [49,50].

Device Stability: The lifetime of the PSCs device is relatively short. Environmental factors such as humidity and heat exposure to these devices may be especially harmful. While encapsulation can reduce the impact of hostile environments, the benefits of small weight, slim profile, and flexibility are still tricky to preserve. Either through extended storage or operation, the device's performance cannot deteriorate significantly with age. Moreover, the extra stable Sn, Ge materials for Pb in perovskite material can improve the overall stability of the perovskite device [51,52].

2.3. Different types of perovskite solar cell

Mesoporous perovskite solar cell (n-i-p), planar perovskite solar cell (n-i-p), and planar perovskite solar cell (p-i-n) are three recent developments in common PSC structures. Light can pass through the transparent conducting layer that is located in front of the ETL in the n-i-p configuration. The p-i-n structures are the opposite arrangement [53].

2.3.1. Mesoporous perovskite solar cell (n-i-p)

The Mesoporous Perovskite Solar Cells (MPSCs) have recently drawn greater interest due to their inexpensive components, simple manufacturing process, and high PCE. In MPSC, a fluorine-doped tin oxide layer (FTO), which typically blocks holes and collects electrons, is placed before the compact layer [1]. Nanoscale pores in the ETL scaffold are a common component of MPSCs [39]. The absorber layer first encases the ETL, creating a tight capping layer, before penetrating it to create an intermixed layer. To complete the device architecture, the top electrode and HTL are sequentially deposited over the absorber layer [37].

The mesoporous layer requires high temperature, which is not desired for scaling-up. The question of whether a mesoporous layer is necessary to increase PCE or improve stability is still up for debate [37]. It is permitted to use the perovskite material to the planner

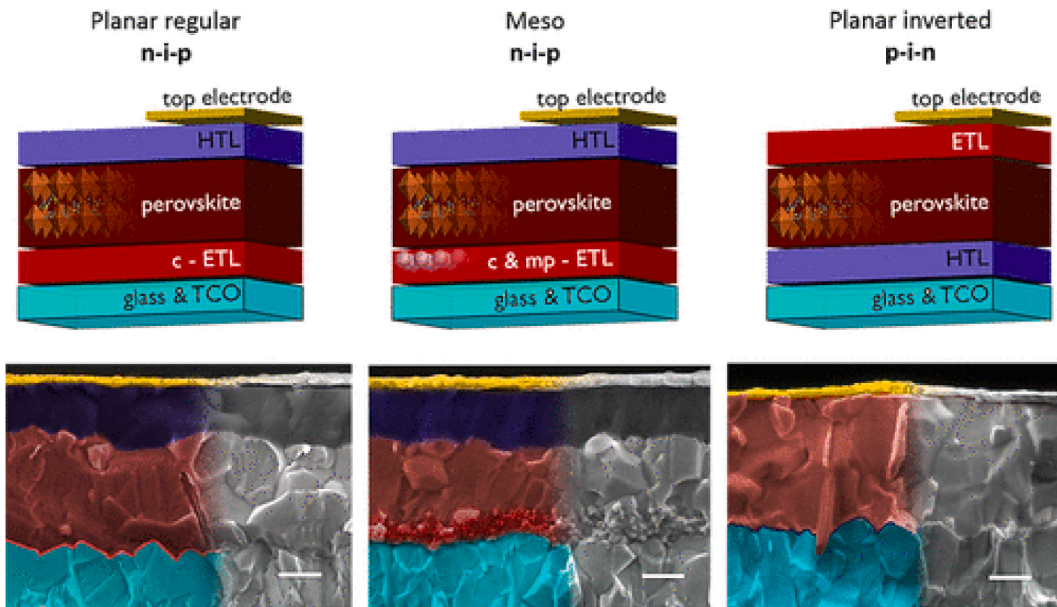


Fig. 6. Schematic diagrams of perovskite solar cells in the (a) n-i-p planar, (b) n-i-p mesoporous (a bilayer structure), (c) p-i-n planar [53], by Saliba et al. reprint with permission.

material in order to enlarge the photosensitive material's receiving light area and produce a more effective PSC, as shown in Fig. 6 [8]. Other mesoscopic metal oxides exist in addition to the most prevalent mesoporous ETM (TiO_2), including Aluminium Oxide (Al_2O_3), ZnO , Tin dioxide (SnO_2), and Zirconium dioxide (ZrO_2).

2.3.2. Regular planar perovskite solar cell ($n\text{-}i\text{-}p$)

Due to their distinctive advantages, including their low-temperature manufacturing technique, low cost, and simple processing, planar perovskite solar cells (PPSCs) have become more attractive [54]. A compact ETM layer distinguishes the planar n-i-p structure from the mesoporous architecture's intermixed layer (perovskite-ETM) [37]. Perovskite/HTL and ETL/Perovskite are the two interfaces. As a result, ETL and HTL effectively and quickly separate the e-h pairs.

2.3.3. Inverted planar perovskite solar cell ($p\text{-}i\text{-}n$)

Due to its many benefits, including simple processing methods, high stability, and minimal hysteresis, PSCs with inverted structure ($p\text{-}i\text{-}n$) have a significant promise for highly effective and adaptable PV devices [1]. Due to the inversion of the extraction layer of a carrier of the n-i-p structure, the planar p-i-n architecture is commonly referred to as an inverted planar structure. A planar structure with a small HTL is frequently used to construct the p-i-n architecture [37]. As both the ETM layer and the HTM layer, inverted structures typically include organic semiconductors, such as [6,6]-Phenyl-C61butyric acid methyl ester (PCBM), Indene-C60 bisadduct (ICBA), C60 SAM, or polyelectrolyte poly [(9, 9-bis(3-(N, N dimethylamino) propyl)-2,7-fluorene]-alt-2,7 (PFN). Every layer in PPSCs effectively affects how well the device performs. Numerous methods were used to improve the inverted PSCs' performance, including controlling the geomorphology, designing a new perovskite composition, and passivation strategies.

Optimizing PSCs inside the lab could waste a massive amount of materials and time; one of the preferred ways to pre-design PSCs is by using modelling and simulation tools to understand the mechanism of improving PSCs performance. Thus, in the next section, we will shed light on the modelling and simulation of PSCs.

2.4. Modelling and simulation of metal-halide perovskite solar cells

2.4.1. Concept

The essential phenomena in photovoltaic devices are explained and made simple by the numerical simulation method, which also determines how the primary parameters affect optimal device output [33,55]. It worth to mention that constructing a solar cell is impracticable without numerical modelling due to higher costs and longer timelines [56]. The method reduces the need for risky assessments of the characteristics of constituent layers and offers a thorough examination of optimizing the solar cell's performance parameters [57]. In addition, using real-world examples from solar cells, the approach is a practical way to assess the importance of various material properties. Furthermore, numerical simulation has become crucial, particularly in the field of material science. It offers insightful suggestions about the known properties of materials. It advances by forecasting the quickest route to discovering new functional materials, which provides guidance for upcoming efforts [58].

The performance of solar cells has been studied using numerical models over the last few years. It was first started by solving Poisson's equation and continuity equations for electrons and holes; Jerry developed an effective analysis technique to analyze the carrier transport problem of silicon solar cells in 1975 [59]. In recent years, several software programs for thin-film solar cells, including SCAPS-1D, PC1D, and AMPS-1D, have been widely utilized to understand the mechanism of solar cells. Many scholars have researched and developed numerical analyses for dye-sensitized solar cells (DSCs). The design of these numerical models has resulted in a better knowledge of the mechanics of solar cells, which adds to the advancement of device efficiency. On the other hand, the operating mechanics of silicon solar cells, DSCs, and perovskite solar cells differ. The performance of silicon solar cells is described using the dopant density and distribution, which is modelled as a p-n junction with doping. The redox level in electrolytes impacts the output voltage of a device in DSCs. Hence it is used to determine the boundary conditions and beginning value. The difference between the quasi-Fermi energy levels for electrons and holes at the two electrodes of the device determines the output voltage in the perovskite model. Thus, carriers' density and potential must be described using the quasi-Fermi energy level model to produce relevant findings. Additionally, the boundary conditions and beginning value must be generated using the quasi-fermi energy level model.

This section provides a numerical model for perovskite solar cells based on Poisson's equation and continuity equations. To decrease the complexity of computing, this model has been reduced as much as feasible within some reasonable assumptions. In addition, this section covers the specifics of computing methodologies and procedures. The simulation findings are obtained using available simulating software. They are utilized to understand how the effective density of state, relative dielectric permittivity and bandgap energy impact perovskite solar cell performance.

2.4.2. Drift diffusion model of current density

The electric current density (current/unit area) in a semiconductor is determined by diffusion and drift processes. Because of the uneven generation of electrons and holes during thermal stimulation or light illumination, carrier density inside the semiconductor is non-uniform. According to Fick's diffusion law, electrons diffuse from higher to lower concentrations. The rate of diffusion of free carriers is proportional to the negative concentration gradient in the substance, according to the law. With a downward concentration gradient, the negative sign vanishes. This denotes that the rate of flow is moving from higher to lower concentrations.

Furthermore, carriers drift due to the effect of the existing electric field. External biasing in a piece of semiconductor or electric field generated across the SCR in a p-n junction causes the electric field to exist across the material. Current densities for electrons (J_e) and holes (J_h) are the sum of individual currents responsible for these mechanisms, as follows:

$$J_e = qn\mu_e E + qD_e \frac{dn}{dx} \quad (2)$$

$$J_h = qn\mu_h E + qD_h \frac{dp}{dx} \quad (3)$$

The μ_e (μ_h) and D_e (D_h) are the mobility and diffusion constants of an electron (hole). The letter E denotes the electric field across the material or device. The first term in the equation is due to the drift process, whereas the second term results from charge carrier diffusion. Electrons drift from a lower to a more significant potential, whereas holes do the opposite. Under the influence of an electric field, an electron drifts with a velocity called drift velocity, which is denoted by v_{edrift} .

$$v_{edrift} = \mu_e E \quad (4)$$

Similarly, holes are drifted with hole drift velocity (v_{hdraft}) under the effect of E, as shown below.

$$v_{hdraft} = \mu_h E \quad (5)$$

In fact, both carriers contribute electric current that flows from higher to lower potential in the same direction. Diffusion of holes from higher concentrations of the hole to higher concentrations of an electron occurs at a p-n junction. On the other hand, diffusion of electrons occurs from a higher concentration of electrons to a higher concentration of holes. As a result, the diffusion directions of electrons and holes are diametrically opposed. These also contribute to the same direction of electric current. The net electric current is the sum of all these individual currents in the same direction.

2.4.3. Basic equations used in simulator

In order to characterize the functionality of perovskite solar cells, a one-dimensional model is constructed in this section utilizing Poisson's equation and continuity equations. Each component layer of the perovskite solar cell, including their energy level, cathode and anode work function, defect density, doping density, etc., affects the device's optoelectronic properties. For the numerical modelling of perovskite solar cells, we used SETFOS-Fluxim, a commercially available piece of software. The influence of absorber layer thickness on the photovoltaic limitations of the perovskite solar cell was therefore studied using the change in perovskite layer thickness. Under equilibrium conditions, the device feature is governed by the equivalent one-dimensional equation. As a result, the equation given below, which describes the relationship between the electric field and charge density [60].

$$\frac{\partial^2 \varphi}{\partial^2 x} = -\frac{\partial E}{\partial x} = -\frac{\rho}{\epsilon_s} = -\frac{q}{\epsilon_s} [p - n + N_D^+(x) - N_A^-(x) \pm N_{\text{def}}(x)] \quad (6)$$

The electrostatic potential is denoted by the symbol φ , charge is denoted by q , static relative permittivity of the medium is denoted by ϵ_s , electrons and holes are denoted by n and p , donor and acceptor densities are denoted by N_D^+ and acceptor densities are denoted by N_A^- , and defect densities of both the acceptor and the donor are denoted by $N_{\text{def}}(x)$. Whereas the carrier continuity equation in the PSC device can be represented as follows,

$$-\frac{\partial j_p}{\partial x} + G - U_p(n, p) = 0 \quad (7)$$

$$\frac{\partial j_n}{\partial x} + G - U_n(n, p) = 0 \quad (8)$$

Where, j_n and j_p are called electron and hole current density, $U_n(n, p)$, $U_p(n, p)$ are recombination rate of electron and hole, and G is carrier generation rate, respectively. Concurrently, the carrier current density is also obtained from the equation below,

$$j_p = qn\mu_p E - qD_p \frac{\partial n}{\partial x} \quad (9)$$

$$j_n = qn\mu_n E + qD_n \frac{\partial p}{\partial x} \quad (10)$$

Where, q is called the charge, μ_p and μ_n is the carrier mobilities and D_p and D_n is the diffusion coefficient of the carriers. At the same time, the numerically simulating software extracts all the solar cell's fundamental equations, namely, the generation, recombination rate, current density, and hole density, respectively. Below the detailed introduction of simulating software of SCAPS-1D softwares has been provided.

2.4.4. Description of SCAPS-1D simulation

A one-dimensional simulation programme called SCAPS-1D was designed at the University of Gent in Belgium. It has been used to research several solar cell types, including CZTS, CdTe, CIGS, etc. [61,62]. When compared to other software, SCAPS-1D features a very user-friendly operation window and a variety of models for grading, faults, and recombination. The primary characteristics of SCAPS-1D, including the properties of the materials and defects, can be defined in seven semiconductor layers. There are numerous grading laws available for almost all parameters of the materials and defects, and the defect definition can be set in both bulk and

interface [63]. The software supports five different defect types and distributions. SCAPS-1D can be used to determine the number of solar cell-related features, including energy bands, concentrations, currents, *J-V* characteristics, C-V, C-f, and QE. Additionally, the program can carry out a wide range of computing and recording activities, including single-shot and batch computation, curve fitting, and data and diagram recording, respectively. The schematic layer diagram is shown in Fig. 7(c–d) while the solar cell parameters and EQE are depicted in Fig. 7(a–b) with the variation of the absorber layer; the structure shown in last figure is a planar n-i-p configuration using SnO_2 and Spiro-OMeTAD as ETL and HTL respectively; added to the double cation as a perovskite layer.

2.5. Fabrication techniques in PSCs

The PSCs' quick increase in PCE from 3.8% to 25.2% within a decade indicates their potential. The approach to efficiency increase included changes to the device architecture, new carrier transport materials (ETLs and HTLs), and improvements to the absorber layer, among other things. The alteration of the anionic and cationic components, such as the use of FA along with MA and mixed halides, improves the absorber layer shown by Eperon et al.; and Aharon et al. [64,65], the addition of the performance booster additives (like Cs and Rb) and improvement in the perovskite film fabrication technique [65]. The structural and optoelectronic characteristics of the film depend on the added solvent, the method used to make the film, the annealing temperature, and environmental factors like temperature, moisture content, oxygen, and others in addition to the organic and inorganic components in the perovskite layer. To design an effective PSC, it is typically necessary to have a tight control over the stoichiometry, grain structure, and crystallographic phase of the perovskite layer [66]. Researchers have conducted extensive research to establish the various fabrication procedures because these characteristics heavily depend on the film deposition technique [67,68]. The various film fabrication and PSC manufacturing methods utilized for mass production are covered in the sections that follow.

The perovskite film's quality has the biggest impact on how well the PSCs perform. To present, a number of techniques have been developed perovskite films of higher quality. The processing methods, which directly affect PSC performance, determine the qualities of the film, such as shape, homogeneity, crystallinity, and phase purity. According to X-ray diffraction research, perovskites have a substantially lower activation energy than silicon ($280\text{--}470 \text{ kJ mol}^{-1}$) [69,70]. Low activation energy means that a number of low-temperature techniques, which are covered in this section, can be used to fabricate the perovskites. The fabrication method must provide total film coverage over the substrate since partial film coverage could result in the development of shunt routes by bringing ETLs and HTLs into direct contact. Second, if the active layer is not completely covered, incoming light may pass through without being absorbed. This section discusses the numerous perovskite-film deposition methods.

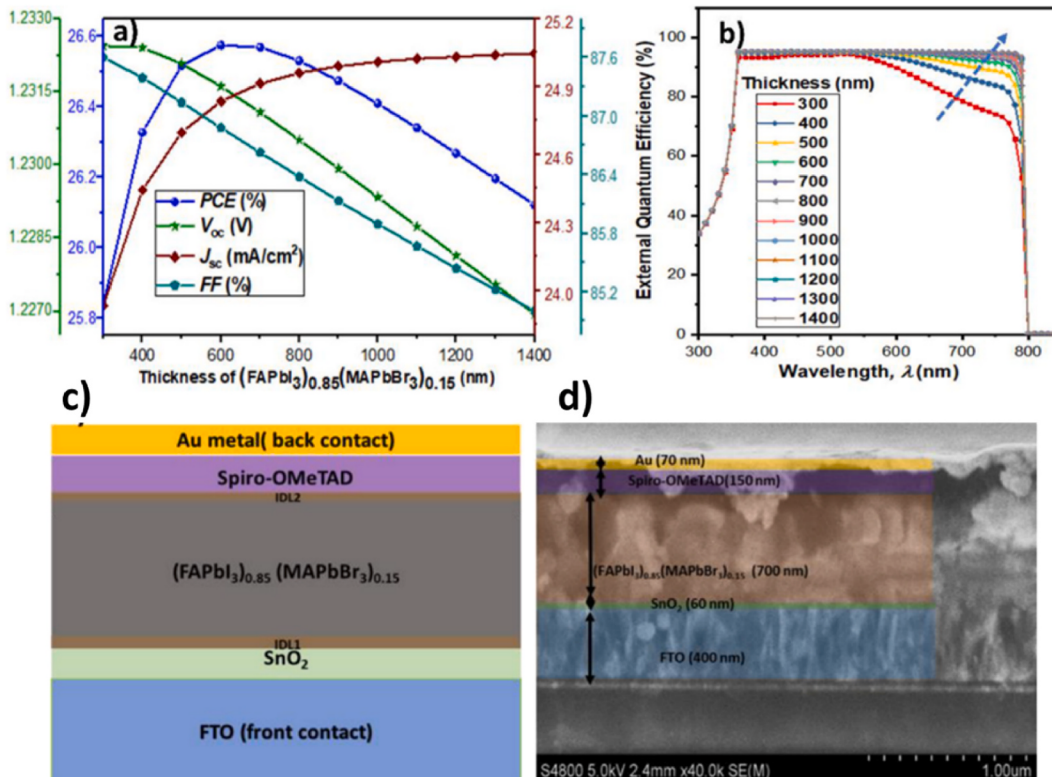


Fig. 7. (a–b) Outputs parameters of *J-V* vs. different perovskite layer thickness. Reprinted with permission from Ref. [53]. (c–d) Schematics layers of the PSC devices for the study of SCAPS -1D. Reprinted with permission from Ref. [60].

2.5.1. Single-step deposition

Because of its ease of use and low cost, this approach is the most popular. In this method, the TiO_2 scaffold is typically spin-coated with the precursor solution. Here, the organic and inorganic solutes are combined in an aprotic polar solvent such as DMF, DMSO, GBL, DMAc, and NMP to produce a precursor solution [71,72]. At room temperature, all of the solvents have a low vapour pressure and a high boiling point. A homogeneous and crystalline layer of perovskite is fabricated as a result of strong ionic interaction between metal cations and halogen anions. The convective self-assembly and solvent evaporation that took place while the material was spinning are what caused a uniform layer to form. After the precursor solution has been spin-coated onto the substrate, the substrate is then heated to between 80 °C and 150 °C for annealing [73]. However, spin coating alone never produces a layer that is uniform and homogenous over a significant surface. According to a study, the TiO_2 layer's thickness affects the homogeneity of the perovskite layer [74]. However, this deposition approach needs fewer processing stages and is, therefore, simpler to carry out, sluggish crystallization results in a non-uniform layer with pinholes. Later, a two-step sequential deposition method was developed to overcome the film's unregulated development and the generated crystals' varied shape [75]. Fig. 8(a) shows a schematic illustration of the One-Step deposition procedure. Mhamdi et al. recently used hybrid perovskite structures made from methylammonium lead bromide solutions that were formed using the one-step spin coating deposition process [76]. The investigation also looked into how the annealing temperature of the MAPbBr_3 films and devices affected them. The features of perovskite films, including as their photoluminescence, crystallinity, and morphology, as well as the functionality of the devices, have been greatly influenced by adjusting the temperature fluctuation. The best device performance is displayed by the 70°C-annealed devices, which have a maximum fill Factor of about 76.5%. The SEM images of FTO/ TiO_2 / MAPbBr_3 (Fig. 8(b–c) below) also provide top view and cross-sectional images [76].

2.5.2. Two-step sequential deposition

Scientists and researchers have demonstrated a new method of deposition techniques following the success of the one-step deposition. The issue with the one-step deposition process is further resolved in this by creating a perovskite layer that has a high surface coverage and demonstrates homogeneity. Liang et al. suggested a two-step solution deposition method to prevent this [77]. By spin coating the DMF solution at a temperature of 70 °C, they first applied a film over the nanoporous TiO_2 layer. After that, the layer underwent a reaction with an MAI solution to become a perovskite layer. The process is as follows; (i) spin coating the MAI solution over the PbI_2 layer and (ii) dip coating the PbI_2 film over the MAI solution, the layer of MAI is added using this technique. When the

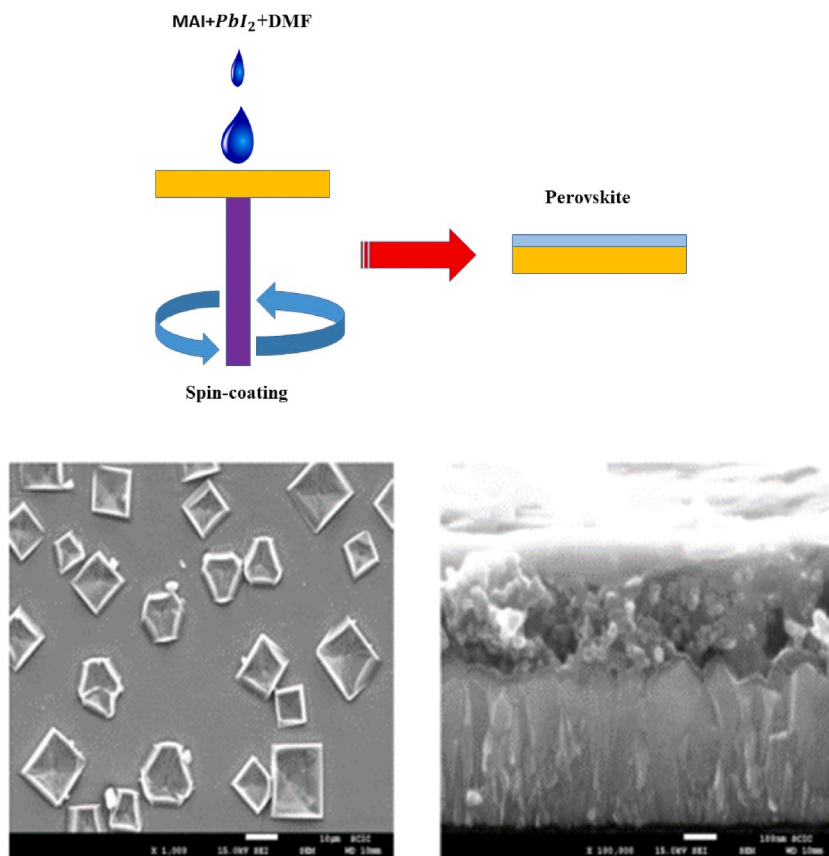


Fig. 8. (a) One step deposition techniques, SEM image of FTO/ TiO_2 / MAPbBr_3 (b) top view image (c) cross-sectional image. Reprinted with permission from Ref. (Mhamdi et al., 2019).

MAI solution is spin-coated over the PbI_2 film, the quality of the perovskite layer produced depends in part on the spinning time and speed. 2018 Chinese et al. [78]. At the same time, the dipping time and dipping concentration are crucial in the case of dip coating the MAI layer. Im et al. investigated the effect of MAI concentration over surface morphology and discovered a relationship showing that the grain size decreases as the MAI concentration rises [79]. This process has some drawbacks while producing superior film than the one-step deposition method. The interaction between surface roughness and particle size is the key downside. The surface roughness rises together with the grain size. A smooth perovskite film with small grain suffers from a short diffusion length and a short carrier lifetime, whereas a rough perovskite film with greater grain size causes high leakage current and significant surface recombination loss. As a result, a suitable composition needs to be fixed. Second, when PbI_2 is partially converted, particularly in planar structures, the remaining PbI_2 lowers light absorption and impairs carrier transport, further impairing the PSCs' performance [80]. Solvent engineering was used in order to address these problems. Fig. 9 shows a schematic illustration of the Two-Step Deposition Technique. Recent research by Mhamdi et al. has also demonstrated that the cells using a two-step procedure have improved in terms of absorbance, film quality, crystallinity, and PCE as depicted in Fig. 10 [81]. The device efficiency increased using the two-step deposition method from 1.9% to 2.4%, with a J_{SC} of 3.134 mA/cm^2 , a V_{OC} of 0.984 V , and an FF of 67.1% with one step and two step deposition processes. The method is among the most effective methods for creating high-performing perovskite solar cell devices.

2.5.3. Thermal evaporation

One of the most recent approaches for fabrication of the perovskite solar cell is the vacuum thermal evaporation. It was firstly introduced by Snaith et al. where he fabricated the first vacuum-deposited film by co-evaporation of the organic and inorganic species [83]. Simultaneously evaporating MAI and PbI_2 precursor salts from various sources at 10^{-2} mbar and depositing them at a 4:1 ratio, they fabricated $\text{CH}_3\text{NH}_3\text{PbI}_{3-x}\text{Cl}_x$. They manufactured the film in the nitrogenous environment of the glove box while placing sensors above the ceramic crucible. While spin coating produced an uneven film covering with crystalline "platelets" in the micron range, vapour deposition produced an incredibly homogeneous film with crystalline features spanning the length scale of 100's of nanometres. The deposition rate of MAI was challenging to regulate with this approach. This could be avoided, though, by using the sequential deposition technique, in which PbI_2 was coated first and then MAI vapour was deposited. Snaith made two cells using both techniques, including solution processing, and found that the PSC made using vapour evaporation performed better. The vapour deposition diagram is illustrated in Fig. 11, where PbX_2 and MAI are both shown graphically and deposited in the film at a high vacuum state.

In recent times the work by Juan et al. achieved an efficiency up to 8.65% using vapour evaporation CsPbBr_3 -based PSC. The J - V curve is depicted in Fig. 11 below [84]. The proportion of the MAI and PbI_2 precursor are shown in the J - V curve, respectively.

It also need to be mentioned that there are multiple fabrication techniques such as Rapid deposition crystallization, Lewis base adduct method of lead (II) iodide, Pulse laser deposition (PLD), etc. These can be efficient for the production of perovskite solar cell devices.

3. Major influential factors in perovskite material in PSCs

Numerous factors affect the overall outcomes in the perovskite solar cell. The few essential physical factors are listed below.

3.1. Impact of solar spectrum

The solar cell efficiency is directly proportional to solar irradiance, which fluctuates with the Sun's position. The Sun's position in relation to the Earth changes throughout the year, depending on the seasons. The Sun is higher in the sky during the summer than it is during the winter. As the season changes from winter to summer, the power received per unit surface area outside the Earth's atmosphere varies from 1.4 kW/m^2 to 1.31 kW/m^2 at the Earth's mean distance from the Sun. The wavelength range of 250 nm–3000 nm accounts for more than 80% of solar electricity. Photons with a wavelength approaching 600 nm have the highest intensity in this solar spectrum. Solar energy must pass through absorption on its path, reaching the Earth.

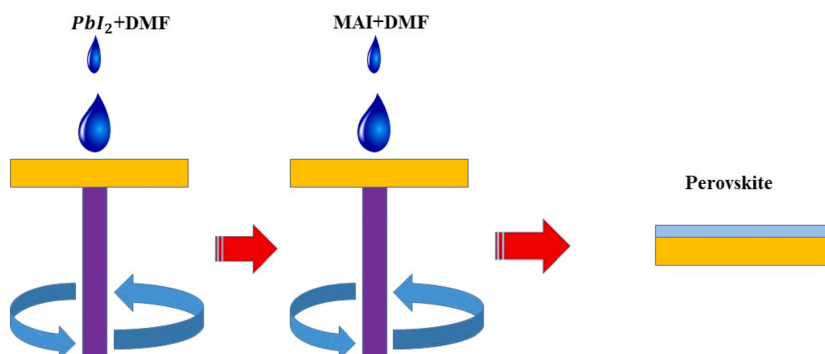


Fig. 9. Schematic representation of Two-Step deposition technique.

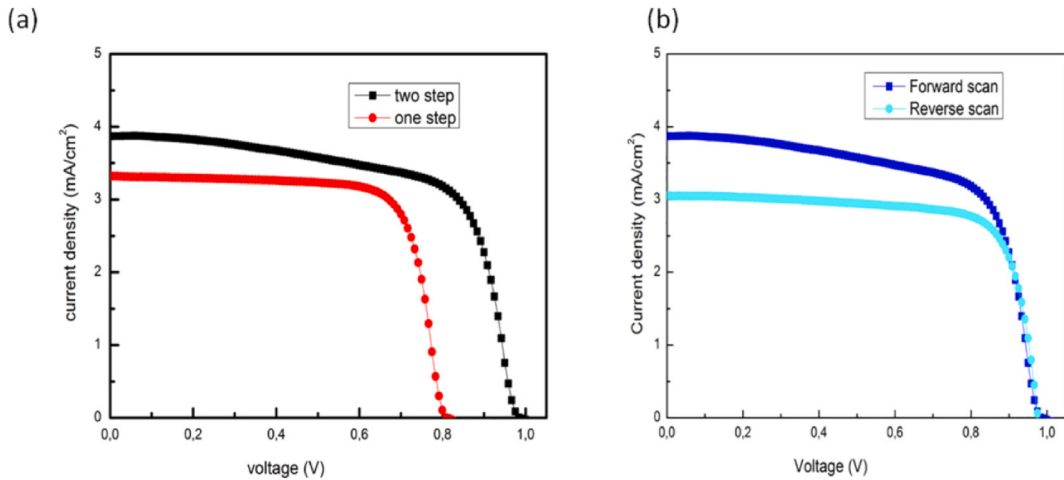


Fig. 10. (a) The photovoltaic performance of CH₃NH₃PbBr₃ solar cells with two deposition procedures, and (b) demonstrates the hysteresis characteristic of MAPbBr₃ solar cells with a two-step spin coating approach. Reprinted with permission from Ref (Mhamdi et al., 2021). [82]. Copyright (2022) Elsevier.

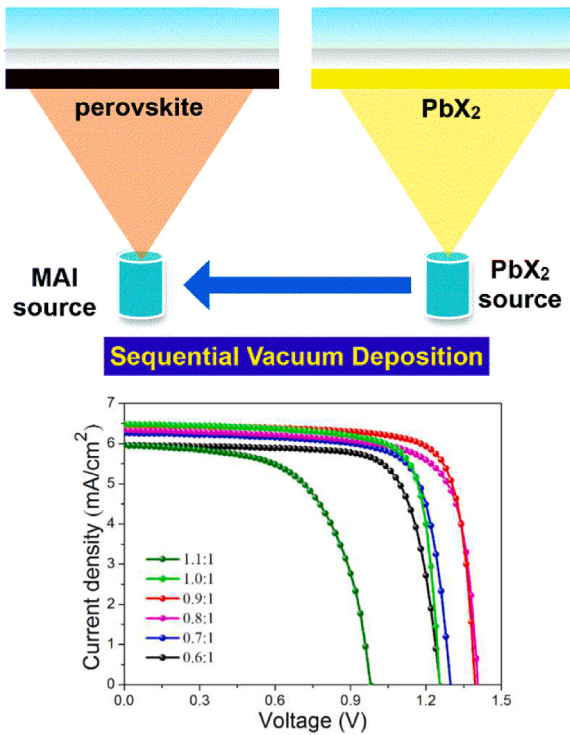


Fig. 11. Schematic representation of the Thermal evaporation techniques and current density (*J*-*V*) value; Reprinted with permission from Ref (Juan et al., 2019).

In addition, the effect of turbidity, ground reaction, and scattering are not negligible in the context. A certain solar spectrum undergoing specific conditions is leveled with an air mass (AM) standard symbol. A conventional technique to characterize the nature of the solar spectrum is to use a simulated result equivalent to Air mass coefficient indicated by a value preceded by the sign AM. After passing through the atmosphere on its path to the planet, the standard AM considers. It's defined as the ratio of solar radiation path length (L_r) to zenith path length (L_z), which is calculated as follows:

$$AM = \frac{L_r}{L_z} \quad (11)$$

The zenith path length is defined in terms of zenith angle (in degree) of the solar radiation (z) as,

$$L_z = L_r \cos(\theta_z) \quad (12)$$

Depending on the solar cell/panel location, different standard solar spectrums can be used to conduct a performance test on it. Some of the standard air mass coefficients are listed below.

- (a) **AM0:** AM0 denotes the sun spectrum outside of the atmosphere. At that point, the actual path length of solar radiation is assumed to be zero. A standard solar spectrum is used in communication satellites for solar cell testing.
- (b) **AM1:** The equator and its environs receive sun radiation with a zenith angle of 0°, resulting in an AM coefficient of 1. The Sun is overhead; therefore, it is a conventional solar spectrum model.
- (c) **AM1.5:** It's the conventional solar spectrum, with $\theta_z = 48.2^\circ$, that's used in solar cell testing on the ground. The majority of the world's population lives in a moderate climate zone between the tropics and the arctic. As a result, the AM standard of such a location was chosen for testing terrestrial solar cells. The newest standard AM1.5 spectrum for solar cell design is ASTMG-173, which assumes a radiation intensity of 1000 W/m^2 . Intensity (I_r) of the solar radiation under different AM spectrums can be approximated using a standard formula as given below.

$$I_r = 1.1 \times I_{ex} \times 0.7AM^{0.678} \quad (13)$$

Fig. 12 displays extra-terrestrial (AM0) and terrestrial (AM1.5) solar spectrum data identified as ETRASTME-490 and ASTMG-173-03, respectively, taken from NREL-2019. The space application needs to operate under AM0 illumination. An analysis of the outputs with the solar spectra of AM0 and AM1.5 spanning the visible spectrum wavelength ranges was done analyzed the effect of Sun illumination using a theoretical approach between Monte- Carlo and drift-diffusion simulation for p-i-n structure based on a new perovskite layer Cs_2CrI_6 with a band gap of 1.08 eV [85]. As illustrated in **Fig. 13**, the photovoltaic parameters of the PSCs under AM0 attained a V_{OC} of 0.698 V, J_{SC} of 47.4 mA/cm^2 , FF of 84.3%, and PCE of 20.4%. While under the illumination of 1.5AM, the parameters of PSCs are V_{OC} of 0.693 V, J_{SC} of 38.3 mA/cm^2 , FF of 84.4%, and PCE of 22.4%, respectively. Additionally, the device's capabilities, such as V_{OC} , show a modest decline even when the radiation's proton fluency surpasses $10^{13} \text{ p.cm}^{-2}$ [85].

3.2. Impact of thickness

One of the most important approaches for The MAPbI_3 -based PSC device is accomplished using the parameters. **Fig. 14** the variation of thickness in the active layer of MAPbI_3 to study the fundamental J-V characteristics of perovskite solar cells. It can be well observed that the short circuit current density (J_{SC}) at 350 nm of PAL obtains a lower value of 6.5 mA/cm^2 , and it monotonically increases to 7.9 mA/cm^2 at the PAL thickness to 600 nm. This can be explained more collectively as the material exposed to light at 600 nm of the PAL is higher; hence, high excitons will be generated. However, with higher thickness than 600 nm, a recombination effect comes to play in the PSC device. The experimentally verified value by Juan et al. has also shown similar outcomes as depicted in **Fig. 14** [84]; in the work, the scanning electron microscopy (SEM) was used to examine the surface morphology of CsPbBr_3 films of various thicknesses. The CsPbBr_3 films are made of dense CsPbBr_3 grains with good homogeneity and full or almost full surface covering. The CsPbBr_3 grain size grows from 350 to 650 nm as the thickness of the CsPbBr_3 film rises, then it reduces as the thickness increases further to 850 nm. This reflects two different pathways for film growth: The film grows from the growth and fusion of existing CsPbBr_3 grains when the thickness is less than 650 nm. Small grains begin to develop on the edges of large grains and their boundaries when the thickness exceeds 650 nm [60,84].

It is worth to mention that changing the perovskite thickness can be released through the molar concentration ratio of the solution or/with deposition parameters such as spin-coating rpm.

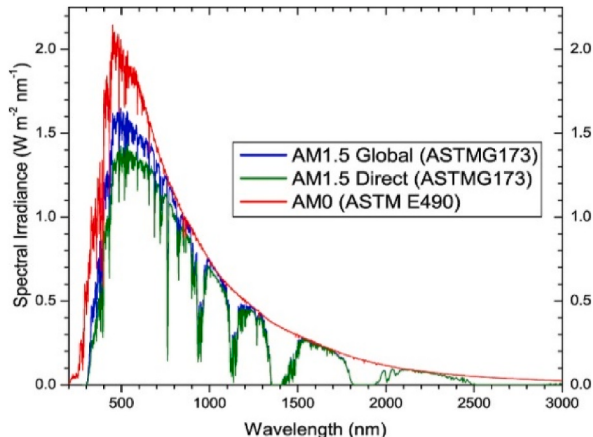


Fig. 12. Comparison between the AM0, AM1, and AM1.5 solar spectrum (from PV education).

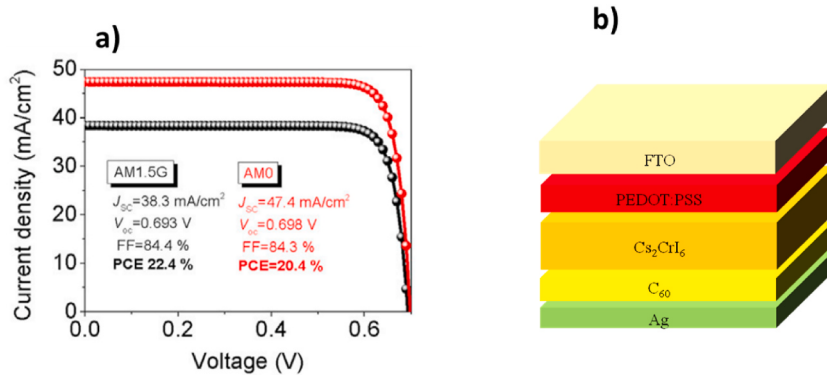


Fig. 13. (a) J - V curves under AM1.5 and AM0 illumination of the simulated perovskite solar cells based on Cs₂CrI₆ as absorber layer, b) the p-i-n structure used for drift-diffusion model [85]. Reprinted with permission from Ref. (Zhao et al., 2019). Copyright (2022) Elsevier.

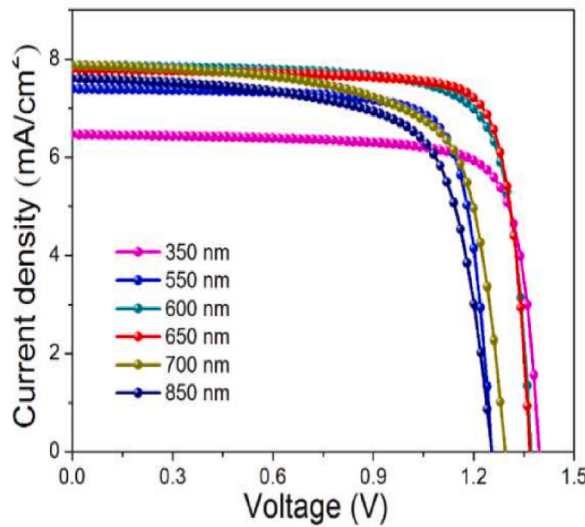


Fig. 14. The comparison of simulation and the experimental reports by Juan et al. with J-V curves of the planar CsPbBr₃ based perovskite solar cells with different CsPbBr₃ film thicknesses [84]. Reprinted with permission from Ref. (Juan et al., 2019).

3.3. Impact of defect density

Another important parameter determines the overall outputs of the perovskite devices. The bulk defect density significantly impacts the performance of perovskite solar cells. Incomplete dangling bonds within the material leads to additional trap energy levels within the bandgap and these levels act as a recombination centre and reduces the carrier lifetime. These defects levels can be passivated by using compositional, chemical, or material engineering to reduce the defect density and increase the carrier lifetime for better performance. In this subsection, details about the impact of bulk defect densities ranging from 1×10^{14} cm⁻³ to 1×10^{17} cm⁻³ in four steps has been provided, depicted in Fig. 15(a). At lower defect density the MASnI₃-based material offers the highest J_{SC} of 27.44 mA/cm², whereas the value keeps decreasing and reaches a minimum value at the defect density level of 5×10^{17} cm⁻³. As the density of flaws significantly influences the values of V_{OC} . An intriguing finding is that while J_{SC} is unaffected by the defect density in this range, V_{OC} declines from 1.15 V to 0.85 V as the defect density rises from 10^{14} to 10^{17} cm⁻³. These findings are consistent with the experimental published data by Santos et al. [86], where a related tendency in theoretical validation may be seen in Fig. 15(b). Further, in Fig. 15(c) the EQE for the device is measured at the defect density level of 1×10^{16} cm⁻³.

3.4. Impact of temperature

Thermal instability is a significant concern for researchers and scientists in PSCs. The fact that annealing is a critical stage in the fabrication of perovskite films indicates that perovskites will likely be exposed to high temperatures. The operating temperature for solar cells ranges from 300 K to 400 K; hence, the newly fabricated perovskite solar cells must be able to tolerate high-temperature

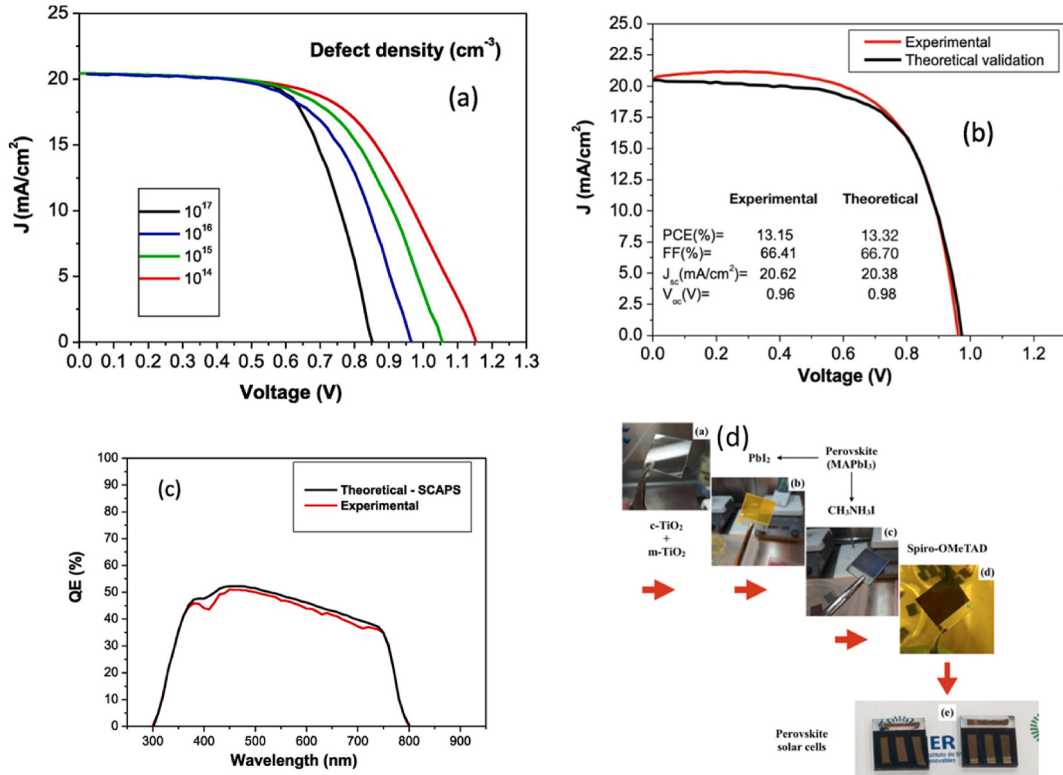


Fig. 15. ((a-d) The J - V solar cell performance parameter over absorber defect density, QE over wavelength and perovskite solar cell fabrication process with reported by Santos et al. [86]. Reprinted with permission from Ref. (Santos et al., 2020); Copyright (2022) Elsevier.

conditions. Previous research has shown that the MAPbI₃ active layer has a very low thermal conductivity [87] and also degrades at a temperature of 85 °C (K) even in an inert atmosphere.

On the contrary, the constituent material in the perovskite structure, in the ABX₃ type of structure, where A is a cation and primarily an organic cation component, is a volatile substance in nature that tends to degrade at high temperatures [88]. Previously, According to Coining et al., heating the perovskite layer in a nitrogenous atmosphere to 85 °C causes it to completely disintegrate into PbI₂ (MA) [89]. This experiment was carried out for 24 h in the dark using pure dry oxygen, pure dry nitrogen, and an ambient atmosphere with 50% relative humidity. Kim et al. investigations of the thermal stability of the MAPbI₃ film at three different temperatures of (i) 25 °C (298 K), (ii) 100 °C (373 K), (iii) 200 °C (473 K) provided additional evidence of this [90]. This concludes that the stable PV cell must possess thermal stability up to 85 °C (358 K) [92]. This further confirmed the fact that with an increase in temperature, MAPbI₃ starts turning into PbI₂ by Kim et al.

It can be observed that the formation energy of MAPbI₃ lies in the range of 0.11 eV–0.14 eV, which is closer to 0.093 eV. This leads to the degradation of MAPbI₃ due to continuous exposure to 85 °C [91]. The decomposing temperature of the perovskites lies between 100 °C (373 K) and 140 °C (413 K) [92]. In order to combat the instability arising due to MA, researchers used more significant cation FA or inorganic Cs instead of MA. Eperon et al. studied the thermal conductivity of FAPbI₃ and MAPbI₃ film by heating them up to 150 °C (423 K) in an open-air condition. This experiment further confirmed that the MAPbI₃ film is transformed into PbI₂ while FAPbI₃ withstood the high temperature of 150 °C (423 K) up to 60 min [65].

The replacement in the perovskite solar cell also improves the optoelectronic characteristics. The efficient replacement of MA organic cation with FA makes the tolerance factor reach 0.99, which can improve thermal stability, as discussed in section 2. Apart from that, various researchers confirm that FAPbI₃ is more thermally stable than any other similar compositional perovskite material [93]. The researchers have also used mixed cation to deal with this issue, which concurrently improves the volatility and instability along with the ions of Caesium and Rubidium [94]. It needs to be mentioned that all inorganic PSCs are also fabricated accordingly to deal with this issue. The crystal structure of CsPbI₃ attains the cubic phase upon annealing at high temperature, i.e., 300 °C (573 K), whereas CsPbBr₃ can be prepared at room temperature and is structurally stable but has a wide bandgap of 2.3 eV [95]. The crystal structure has an impactful influence on the electronic properties of the perovskite material. In the MAPbI₃ material, a tetragonal phase generally exists at room temperature. At a higher temperature range, symmetry increases, and crystal structure exhibits a cubic phase. In contrast, at a lower temperature, the symmetry is reduced to the orthorhombic phase, as confirmed by Baikie et al. [96]. Therefore, the PSCs based on MAPbI₃ have a minor harmful impact on performance due to the lattice distortion.

Spiro-OMeTAD, on the other hand, is the HTL that is most frequently utilized because of its excellent opto-electrical properties and band alignment with perovskites. This is one of the causes of the PSCs' heat deterioration. The interfaces and the contact between the

absorber layer and HTL are affected because the Spiro-OMeTAD tends to crystallize at a higher temperature. Additionally, the perovskite layer is oxidized by the component in this material, 4-*tert*-butylpyridine (TBP) [97]. Thirdly, the Spiro-OMeTAD is a little bit expensive for large-scale fabrication. The recent outcomes by Vinod et al. outshined the stability of Spiro-OMeTAD-based PSC by using an inorganic hole transport layer, copper (I) thiocyanate (CuSCN), and cuprous iodide [98]. They used a quick solvent removal technique, producing a homogeneous CuSCN layer that sped up the extraction and collection of carriers. The use of copper (I) thiocyanate (CuSCN) as an efficient HTL in the PSC, which demonstrated excellent thermal stability during prolonged heating, was also further supported by Arora et al. The device successfully retained 95% of PCE after a 1000-h test at 60 °C with one sun lighting scenario (Arora et al., 2017). Leo et al. employed carbon as a back electrode and zirconium oxide (ZrO) as the HTL, achieving more excellent thermal stability. The device was exposed to the harsh summer weather for a week, and an unexpectedly stable operation was achieved [99]. To solve these issues, the inorganic HTL was employed with some additives, and HTL-free PSCs were fabricated [100]. Such modification has the potential to enhance the device performance and stability. Khatiwada et al. found the temperature dependency on perovskite J-V characteristics as shown in Fig. 16 [101].

3.5. Moisture and oxygen effect

The first problem PSCs encounter is the perovskite layer's interaction with oxygen and water molecules. This is an inevitable occurrence that happens even when cells are being tested and put together. When water molecules react with the ABX₃ layer, i.e., MAPbX₃, the layer separates into its component parts. Taking MAPbI₃ layer as a standard example, the breakdown route is explored. It first degrades into the original MAI and PbI₂, then creates aqueous HI, solid PbI₂, and volatile CH₃NH₂ as a result [102]. The hygroscopic nature of the amine salts generally causes the instability caused by moisture. In the presence of moisture, the behavior of MAPbI_{3-x}Cl_x and MAPbI₃ is similar: MA sublimates, leaving just PbI₂ remaining [92]. The substance is hydrophilic, which causes it to rapidly absorb water from its environment and result in the fabrication of compounds that resemble hydrates (CH₃NH₃)₄PbI₆·2H₂O) [103].

The degradation pathway was previously illustrated by Zhang et al. in the year of 2018 [95]. According to the theory, water molecules act as a catalyst for deterioration. When exposed to ambient conditions, the perovskite film often changes from a dark brown colour to a light-yellow tint. The crystal structure affects the perovskite film's optoelectronic characteristics. Phase transformation in perovskite causes the crystal structure to be distorted, which lowers the efficiency of the cell. This fact was confirmed in more detail when Jeffrey A. Christians et al. showed that altering the crystal structure has a significant impact on the cell's stability and the existence of constituent layers around the perovskite layer. Compared to Spiro-OMeTAD and PTAA, utilizing a material such as HTL with hydrophobic qualities will increase stability. Stability can be improved by covering the cell with a hydrophobic layer. In this instance, Polytetrafluoroethylene coating was utilized by Hwang et al. to obtain increased stability, and they reported minimal degradation for up to 30 days in an ambient atmosphere [104]. According to Naghadeh et al., perovskite film exposure to heat and moisture causes quick disintegration via the removal of the organic component (such as MA), leaving only traces of PbI₂ from the crystal structure [105]. Using the 2D hybrid perovskite [(PEA)₂(MA)₂(Pb₃I₁₀)] with PEA being C₆H₅(CH₂)₂NH₃, Karunadasa et al. In comparison to MAPbI₃, they obtained higher stability after spin-coating the film in the open air. Even 46 days later, the master film still had its crystal structure, but MAPbI₃ entirely decayed [106].

3.6. Other factors

Few more parameters, in addition to illumination, width, bulk defect density, temperature, moisture, and oxygen effect, the layered additives, charge-selective contacts, interfaces (ETL and HTL/perovskite), manufacturing methods, and electrical biasing are some of them [51]. Due to the strong ionic conductivity and low Frenkel and Schottky defect generation energies, the behavior of PSCs under electrical bias is a cause for worry. According to several theoretical research, the vacancy enhanced FA⁺, MA⁺, and ion movement. The ions' low activation energies, which range from 0.1 to 0.8 eV, are equivalent to the energies of the ions in conductors [107]. These ions can readily aggregate and migrate at the perovskite/contact interface under biased conditions, which lowers the internal potential and charge collection efficiency [108]. The hybrid organic-inorganic perovskites have ionic characteristics and low ion migration activation energy.

Moreover, the rate of ionic migration increases as external electric bias, temperature stress, and illumination increase as the ion arrives at the contact between the perovskite layer and the metal electrode after migrating through the perovskite layer. In contrast, the ion immigration is not an issue with silicon or other photosensitive materials. The proper charge collection depends heavily on the contact between the absorber layer and the charge transport layers. It is a deciding factor for any PSC's performance. At the junction of ETL/perovskite and HTL/perovskite, the hydrophilic property of the perovskite layer disrupts the tetragonal crystal structure and produces pinholes and abnormalities. These imperfections could also act as recombination sites, lowering the carrier charge density. Al₂O₃ was placed as a buffer layer to get around this problem [109].

The trapped charge can set off the moisture-induced deterioration at the contact. In a PSC with the following configuration: ITO/PEDOT: PSS/MAPbI₃/PCBM/Al, Xiang et al. analyzed the interfacial degradation and discovered that deterioration occurs at the MAPbI₃ and PCBM interface. They presented a relatively stable device by including TiO₂ nanoparticles into the MAPbI₃/PCBM interface. The device functioned by holding onto 75% of the initial PCE for 200 h [110]. While Liang Xu et al. conducted a theoretical analysis to modify the electronic features of the transport layer, such as defect density, doping concentration, and electronic level placement, to reduce performance deterioration caused by interfacial recombination in PSCs. To achieve good PCE, they advised selecting a transport layer with a suitable band diagram instead of passivating the interface flaws. They also offered advice on how to

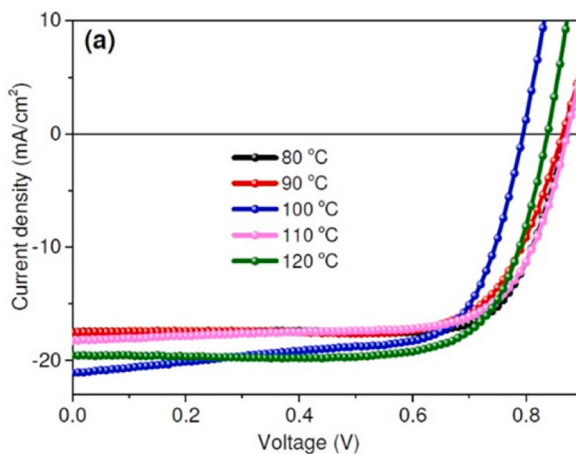


Fig. 16. Effect of different heating temperatures on the performance of perovskite solar cell. Reprinted with permission from Ref (Khatiwada et al., 2015). [101].

construct transport layers properly for a high PCE [111]. The alteration of the film fabrication method can also enhance device performance by Liu et al., in the year of 2017 [112].

Additionally, the device demonstrated improved stability by maintaining 10% of the initial PCE after 1000 h [113]. Cesium lead triiodide (CsPbI_3) can be stabilized in order to make it a more effective solar absorber, according to Steele et al. Although it is quite unstable, CsPbI_3 is one of the materials with promise for solar power applications. These yellow-colored crystals typically don't form perovskite structures at ambient temperature. They joined the thin film of PSC with a glass sheet to colour them black for enhanced absorption. To improve the film's expansion and adherence to the glass, it was annealed at 330 °C [114]. This alteration allowed CsPbI_3 to maintain its black hue and stability at room temperature. When the Bidentate (Bpy) and Tridentate (Tpy) additive were added to PSC, the PCE increased, but the outcome was unsatisfactory when Monodentate Pyridine was added (py). Tridentate (Tpy) and bentate (Bpy) as additions increased grain size and prolonged carrier lifetime [115]. Therefore, all of these studies indicated that choosing the right additives and treating the material properly might improve the functionality and stability of a device, whereas choosing the wrong additives could have the opposite effect.

With this adjustment, both records showed that the open-circuit voltage (VOC) was 5.3 V and the PCE was 21.3%. Both flexible modules and big area cells can benefit from this improvement as depicted by Huang et al. [78]. With the use of interface engineering, Grancini et al. reported an ultra-stable PSC [116]. Using a carbon electrode, they produced a 2D/3D perovskite junction ($\text{HOOC}(\text{CH}_2)_4\text{NH}_3)_2\text{PbI}_4/\text{CH}_3\text{NH}_3\text{PbI}_3$ and fabricated HTM-free modules and PSCs. In mesoporous architecture and carbon-based architecture, respectively, an efficiency of 12.9% and 14.6% was reached. Utilizing a completely printed industrial scale technology, the capacity for large-scale production was also investigated. A 10×10 cm solar module with a high efficiency of 11.2% was achieved. The PSC demonstrated consistent performance for more than 400 days with no change in the percentage of efficiency. In a regulated atmosphere with the presence of moisture and oxygen, these research teams fabricated a fully printed, affordable, and effective PV module with an active area of 50 cm² and a module area of 100 cm². They asserted that the 2D perovskite served as a protective window to keep out moisture, preserving the 3D perovskites and adding to the stability of the device [116].

4. Future challenges

The performance of the device, cost, and stability are the three determining elements for a solar cell's commercial viability. At this time, maintaining long-term stability at the module level and ensuring reliable outdoor operation is the biggest difficulty facing PSCs. The community of perovskite photovoltaics must come to an agreement on the stability measuring methodologies and publish standardised testing procedures. In order to accurately anticipate the lifespan of PSCs under operating settings, new methods need be developed to speed up the ageing process. The performance decay brought on by illumination and heat should be addressed through the design of stable materials and interfaces, even though the deterioration of the perovskite absorber brought on by moisture or oxygen in ambient air can be prevented by the use of suitable encapsulations.

Compositional engineering is considered a pre-step before the fabrication process of solar cells; thus, new machine learning techniques added to robotized synthesis will automate the process toward scaling up PSCs. The lifespan and efficiency of solar panels significantly impact cost per kilowatt-hour. The availability of abundance and cheap raw materials of PSC processing leads to cutting manufacturing costs below those of traditional PV systems. Indeed, PSCs become commercially competitive due to the lower production cost, which can eventually decrease the cost of the whole module, thus; reducing the Levelized cost of electricity (LCOE).

5. Conclusion

The present study provides a detailed view of the perovskite solar cell that can be recommended for future work on the device. Regardless of the wide variation in perovskite solar cell stability and performance due to materials and methods, several key aspects of the rich and varied optoelectronic response of perovskite solar cells (PSC) are generally reproduced pointed to the underlying device operation mechanisms. In this paper, a detailed description of the perovskite materials, their type, simulation and fabrication processes, are also included. Moreover, the major influential factors are also briefly reviewed, such as solar spectrum, thickness, defect density, temperature, and moisture and oxygen effect. These approaches attempt to improve the solar cell current density, open-circuit voltage, light absorption, surface recombination, and effective temperature for solar cell design. The opportunities for future work in each area are also identified, summarized, and discussed in the paper.

Declaration of competing interest

The authors declare that they have no known competing financial interests or personal relationships that could have appeared to influence the work reported in this paper.

Data availability

Data will be made available on request.

References

- [1] A. Louwen, et al., A cost roadmap for silicon heterojunction solar cells, *Sol. Energy Mater. Sol. Cell.* 147 (2016) 295–314.
- [2] E. Radziszewska, The effect of temperature on the power drop in crystalline silicon solar cells, *Renew. Energy* 28 (1) (2003) 1–12.
- [3] H.-S. Kim, S.H. Im, N.-G. Park, Organolead halide perovskite: new horizons in solar cell research, *J. Phys. Chem. C* 118 (11) (2014) 5615–5625.
- [4] N.-G. Park, Organometal perovskite light absorbers toward a 20% efficiency low-cost solid-state mesoscopic solar cell, *J. Phys. Chem. Lett.* 4 (15) (2013) 2423–2429.
- [5] H.J. Snaith, Perovskites: the emergence of a new era for low-cost, high-efficiency solar cells, *J. Phys. Chem. Lett.* 4 (21) (2013) 3623–3630.
- [6] G.C. Lisenky, F. Dauzvardis, M.M.K. Young, Periodic properties illustrated by $\text{CH}_3\text{NH}_3\text{PbI}_3(1-x\text{Br}x)3$ solid solution perovskite semiconductors, *J. Chem. Educ.* 98 (7) (2021) 2392–2397.
- [7] T. Oku, et al., *Fabrication and Characterization of $\text{CH}_3\text{NH}_3\text{PbI}_3$ perovskite solar cells Added with polysilanes*, *Int. J. Photoenergy* 2018 (2018), 8654963.
- [8] A. Kojima, et al., Organometal halide perovskites as visible-light sensitizers for photovoltaic cells, *J. Am. Chem. Soc.* 131 (17) (2009) 6050–6051.
- [9] S. Yang Woon, et al., Iodide management in formamidinium-lead-halide-based perovskite layers for efficient solar cells, *Science* 356 (6345) (2017) 1376–1379.
- [10] S. Abdelaziz, et al., Investigating the performance of formamidinium tin-based perovskite solar cell by SCAPS device simulation, *Opt. Mater.* 101 (2020), 109738.
- [11] S. Bhattacharai, T.D. Das, Optimization of carrier transport materials for the performance enhancement of the MgAl_3 based perovskite solar cell, *Sol. Energy* 217 (2021) 200–207.
- [12] Y. Raoui, et al., Performance analysis of MAPbI_3 based perovskite solar cells employing diverse charge selective contacts: simulation study, *Sol. Energy* 193 (2019) 948–955.
- [13] A. Hima, et al., An optimized perovskite solar cell designs for high conversion efficiency, *Superlattice. Microst.* 129 (2019) 240–246.
- [14] S. Srivastav, et al., Comparative Performance Analysis of Lead-Free Perovskites Solar Cells by Numerical Simulation, 2021.
- [15] Y. Reyna, et al., Performance and stability of mixed $\text{FAPbI}_3(0.85)\text{MAPbBr}_3(0.15)$ halide perovskite solar cells under outdoor conditions and the effect of low light irradiation, *Nano Energy* 30 (2016) 570–579.
- [16] D. Muchahary, et al., A brief on emerging materials and its photovoltaic application, in: L.R. Thoutam, S. Tayal, J. Ajayan (Eds.), *Emerging Materials: Design, Characterization and Applications*, Springer Nature Singapore, Singapore, 2022, pp. 361–406.
- [17] S. Bhattacharai, et al., Investigation of carrier transport materials for performance assessment of lead-free perovskite solar cells, *IEEE Trans. Electron. Dev.* 69 (6) (2022) 3217–3224.
- [18] D. Liu, J. Yang, T.L. Kelly, Compact layer free perovskite solar cells with 13.5% efficiency, *J. Am. Chem. Soc.* 136 (49) (2014) 17116–17122.
- [19] D.-H. Kang, N.-G. Park, On the current-voltage hysteresis in perovskite solar cells: dependence on perovskite composition and methods to remove hysteresis, *Adv. Mater.* 31 (2019), 1805214.
- [20] J. Li, et al., Biological impact of lead from halide perovskites reveals the risk of introducing a safe threshold, *Nat. Commun.* 11 (1) (2020) 310.
- [21] Y. Kuang, et al., Enhanced optical absorption in perovskite/Si tandem solar cells with nanoholes array, *Nanoscale Res. Lett.* 15 (1) (2020) 213.
- [22] M. Moreira, et al., Structural and optical properties of CaTiO_3 perovskite-based materials obtained by microwave-assisted hydrothermal synthesis: an experimental and theoretical insight, *Acta Mater.* 57 (2009).
- [23] L. Lin, et al., Inorganic electron transport materials in perovskite solar cells, *Adv. Funct. Mater.* 31 (2021), 2008300.
- [24] Arandiyian, H.J.M.C.O.L.-b.P.M.O., *Methane Combustion over Lanthanum-Based Perovskite Mixed Oxides*, 2015.
- [25] S. Mariotti, Hybrid and Inorganic Plumbo-Halide Perovskites for Solar Cells, 2020.
- [26] W. Travis, et al., On the application of the tolerance factor to inorganic and hybrid halide perovskites: a revised system, *Chem. Sci.* 7 (7) (2016) 4548–4556.
- [27] A. Surrente, M. Baranowski, P. Plochocka, Perspective on the physics of two-dimensional perovskites in high magnetic field, *Appl. Phys. Lett.* 118 (17) (2021), 170501.
- [28] L. Protesescu, et al., Nanocrystals of cesium lead halide perovskites (CsPbX_3 , X= Cl, Br, and I): novel optoelectronic materials showing bright emission with wide color gamut 15 (6) (2015) 3692–3696.
- [29] Y. Jiang, et al., Post-annealing of MAPbI_3 perovskite films with methylamine for efficient perovskite solar cells, *Mater. Horiz.* 3 (6) (2016) 548–555.
- [30] D. Weber, $\text{CH}_3\text{NH}_3\text{PbX}_3$, ein Pb(II)-System mit kubischer Perowskitstruktur/ $\text{CH}_3\text{NH}_3\text{PbX}_3$, a Pb(II)-System with Cubic Perovskite Structure, *Z. Naturforsch. B Chem. Sci.* 33 (12) (1978) 1443–1445.
- [31] E. Serpetzoglou, et al., Improved carrier transport in perovskite solar cells probed by femtosecond transient absorption spectroscopy, *ACS Appl. Mater. Interfaces* 9 (50) (2017) 43910–43919.
- [32] P. Bhatt, et al., Investigating the charge carrier transport within the hole-transport material free perovskite solar cell processed in ambient air, *Sol. Energy Mater. Sol. Cell.* 140 (2015) 320–327.
- [33] F. Azri, et al., Electron and hole transport layers optimization by numerical simulation of a perovskite solar cell, *Sol. Energy* (2019) 181.
- [34] J. Kim, et al., A Cu 20 –CuSCN nanocomposite as a hole-transport material of perovskite solar cells for enhanced carrier transport and suppressed interfacial degradation, *ACS Appl. Energy Mater.* 3 (8) (2020) 7572–7579.

- [35] D. Glowienka, et al., Role of surface recombination in perovskite solar cells at the interface of HTL/CH₃NH₃PbI₃, *Nano Energy* 67 (2020), 104186.
- [36] W. Tress, et al., The role of the hole-transport layer in perovskite solar cells - reducing recombination and increasing absorption, in: 2014 IEEE 40th Photovoltaic Specialist Conference (PVSC), 2014.
- [37] K. Mahmood, S. Sarwar, M.T. Mehran, Current status of electron transport layers in perovskite solar cells: materials and properties, *RSC Adv.* 7 (28) (2017) 17044–17062.
- [38] J. Kim, K.S. Kim, C.W. Myung, Efficient electron extraction of SnO₂ electron transport layer for lead halide perovskite solar cell, *npj Computational Materials* 6 (1) (2020) 100.
- [39] M.A. Zaman, M. Akhteruzzaman, M.J. Rashid, Influence of electron transport layer on the performance of perovskite solar cell, in: 2019 2nd International Conference on Innovation in Engineering and Technology (ICIET), 2019.
- [40] Y. Chen, et al., Large-area perovskite solar cells – a review of recent progress and issues, *RSC Adv.* 8 (2018) 10489–10508.
- [41] N.K. Kumawat, D. Gupta, D. Kabra, Recent advances in metal halide-based perovskite light-emitting diodes, *Energy Technol.* (2017).
- [42] J.-H. Lee, et al., ITO and electron transport layer-free planar perovskite solar cells on transparent Nb-doped anatase TiO₂-x electrodes, *J. Alloys Compd.* 845 (2020), 155531.
- [43] X. Xie, et al., Tuning the work function of indium-tin-oxide electrodes for low-temperature-processed, titanium-oxide-free perovskite solar cells, *Org. Electron.* 44 (2017) 120–125.
- [44] A. Assi, W. Rashid Saleh, E. Mohajerani, Effect of metals (Au, Ag, and Ni) as cathode electrode on perovskite solar cells, *IOP Conf. Ser. Earth Environ. Sci.* (2021) 722.
- [45] S. Sirotinskaya, R. Schmeichel, N. Benson, Influence of the cathode microstructure on the stability of inverted planar perovskite solar cells, *RSC Adv.* 10 (40) (2020) 23653–23661.
- [46] M.I. Ahmed, A. Habib, S.S. Javaid, Perovskite solar cells: potentials, challenges, and opportunities, *Int. J. Photoenergy* 2015 (2015), 592308.
- [47] A. Manzi, et al., Resonantly enhanced multiple exciton generation through below-band-gap multi-photon absorption in perovskite nanocrystals, *Nat. Commun.* 9 (1) (2018) 1518.
- [48] C. La-o-vorakiat, et al., Elucidating the role of disorder and free-carrier recombination kinetics in CH₃NH₃PbI₃ perovskite films, *Nat. Commun.* 6 (1) (2015) 7903.
- [49] N.-G. Park, Methodologies for high efficiency perovskite solar cells, *Nano Convergence* 3 (1) (2016) 15.
- [50] W. Huang, et al., Stabilizing high efficiency perovskite solar cells with 3D-2D heterostructures, *Joule* 4 (5) (2020) 975–979.
- [51] M.I. Asghar, et al., Device stability of perovskite solar cells – a review, *Renew. Sustain. Energy Rev.* 77 (2017) 131–146.
- [52] L. Duan, A. Uddin, Defects and stability of perovskite solar cells: a critical analysis, *Mater. Chem. Front.* (2022).
- [53] Y. Raoui, et al., Energy level engineering of charge selective contact and halide perovskite by modulating band offset: mechanistic insights, *J. Energy Chem.* 54 (2021) 822–829.
- [54] S. Bhattacharai, et al., A novel graded approach for improving the efficiency of Lead-Free perovskite solar cells, *Sol. Energy* 244 (2022) 255–263.
- [55] D. Liu, T.L. Kelly, Perovskite solar cells with a planar heterojunction structure prepared using room-temperature solution processing techniques, *Nat. Photonics* 8 (2) (2014) 133–138.
- [56] M. Ebner, et al., Visualization and quantification of electrochemical and mechanical degradation in Li ion batteries 342 (6159) (2013) 716–720.
- [57] T. Minemoto, M.J.C.P. Murata, Impact of work function of back contact of perovskite solar cells without hole transport material analyzed by device simulation 14 (11) (2014) 1428–1433.
- [58] C. Catlow, et al., Advances in computational studies of energy materials 368 (1923) (2010) 3379–3456.
- [59] J.G. Fossum, Computer-aided numerical analysis of silicon solar cells, *Solid State Electron.* 19 (4) (1976) 269–277.
- [60] S. Bhattacharai, A. Sharma, T.D. Das, Factor affecting the performance of perovskite solar cell for distinct MAPI layer thickness, *AIP Conf. Proc.* 2269 (1) (2020), 030071.
- [61] F.A. Jhuma, M.J. Rashid, Simulation study to find suitable dopants of CdS buffer layer for CZTS solar cell, *Journal of Theoretical and Applied Physics* 14 (1) (2020) 75–84.
- [62] M. Burgelman, et al., Modeling thin-film PV devices, *Prog. Photovoltaics Res. Appl.* 12 (2004) 143–153.
- [63] M. Burgelman, J. Marlein, Analysis of graded band gap solar cells with SCAPS, *Proceedings of the 23rd European Photovoltaic Conference* (2008).
- [64] S. Aharon, et al., Temperature dependence of hole conductor free formamidinium lead iodide perovskite based solar cells, *J. Mater. Chem.* 3 (17) (2015) 9171–9178.
- [65] G.E. Eperon, et al., Formamidinium lead trihalide: a broadly tunable perovskite for efficient planar heterojunction solar cells, *Energy Environ. Sci.* 7 (3) (2014) 982–988.
- [66] N.J. Jeon, et al., Compositional engineering of perovskite materials for high-performance solar cells, *Nature* 517 (7535) (2015) 476–480.
- [67] C.-H. Chiang, J.-W. Lin, C.-G. Wu, One-step fabrication of a mixed-halide perovskite film for a high-efficiency inverted solar cell and module, *J. Mater. Chem.* 4 (35) (2016) 13525–13533.
- [68] M. Saliba, et al., How to make over 20% efficient perovskite solar cells in regular (n-i-p) and inverted (p-i-n) architectures, *Chem. Mater.* 30 (13) (2018) 4193–4201.
- [69] D.T. Moore, et al., Crystallization kinetics of organic–inorganic trihalide perovskites and the role of the lead anion in crystal growth, *J. Am. Chem. Soc.* 137 (6) (2015) 2350–2358.
- [70] U. Köster, Crystallization of amorphous silicon films, *Phys. Status Solidi* 48 (2) (1978) 313–321.
- [71] K.L. Gardner, et al., Nonhazardous solvent systems for processing perovskite photovoltaics, *Adv. Energy Mater.* 6 (14) (2016), 1600386.
- [72] N.K. Noel, et al., A low viscosity, low boiling point, clean solvent system for the rapid crystallisation of highly specular perovskite films, *Energy Environ. Sci.* 10 (1) (2017) 145–152.
- [73] X. Sun, et al., Mixed-solvent-vapor annealing of perovskite for photovoltaic device efficiency enhancement, *Nano Energy* 28 (2016) 417–425.
- [74] G.E. Eperon, et al., Morphological control for high performance, solution-processed planar heterojunction perovskite solar cells, *Adv. Funct. Mater.* 24 (1) (2014) 151–157.
- [75] L. Zheng, et al., Morphology control of the perovskite films for efficient solar cells, *Dalton Trans.* 44 (23) (2015) 10582–10593.
- [76] A. Mhamdi, et al., One-step methylammonium lead bromide films: effect of annealing treatment, *J. Mol. Struct.* 1192 (2019) 1–6.
- [77] K. Liang, D.B. Mitzi, M.T. Prikas, Synthesis and characterization of Organic–Inorganic perovskite thin films prepared using a versatile two-step dipping technique, *Chem. Mater.* 10 (1) (1998) 403–411.
- [78] F. Huang, et al., From scalable solution fabrication of perovskite films towards commercialization of solar cells, *Energy Environ. Sci.* 12 (2) (2019) 518–549.
- [79] J.-H. Im, et al., Growth of CH₃NH₃PbI₃ cuboids with controlled size for high-efficiency perovskite solar cells, *Nat. Nanotechnol.* 9 (2014).
- [80] Y. Wu, et al., Retarding the crystallization of PbI₂ for highly reproducible planar-structured perovskite solar cells via sequential deposition, *Energy Environ. Sci.* 7 (9) (2014) 2934–2938.
- [81] H. Mehdi, et al., MAPbBr₃ perovskite solar cells: via a two-step deposition process, *RSC Adv.* 9 (2019) 12906–12912.
- [82] A. Mhamdi, et al., Effect of deposition methods on the optical and morphological properties of CH₃NH₃PbBr₃ inverted solar cells, *Mater. Lett.* 293 (2021), 129742.
- [83] M. Liu, M.B. Johnston, H.J. Snaith, Efficient planar heterojunction perovskite solar cells by vapour deposition, *Nature* 501 (7467) (2013) 395–398.
- [84] J. Li, et al., Fabrication of efficient CsPbBr₃ perovskite solar cells by single-source thermal evaporation, *J. Alloys Compd.* 818 (2020), 152903.
- [85] P. Zhao, et al., A new all-inorganic vacancy-ordered double perovskite Cs₂CrI₆ for high-performance photovoltaic cells and alpha-particle detection in space environment, *Materials Today Physics* 20 (2021), 100446.
- [86] I. Montoya De Los Santos, et al., Optimization of CH₃NH₃PbI₃ perovskite solar cells: a theoretical and experimental study, *Sol. Energy* 199 (2020) 198–205.
- [87] A. Pisoni, et al., Ultra-low thermal conductivity in organic–inorganic hybrid perovskite CH₃NH₃PbI₃, *J. Phys. Chem. Lett.* 5 (14) (2014) 2488–2492.

- [88] A.R.B.M. Yusoff, M.K. Nazeeruddin, Organohalide lead perovskites for photovoltaic applications, *J. Phys. Chem. Lett.* 7 (5) (2016) 851–866.
- [89] B. Conings, et al., Intrinsic thermal instability of methylammonium lead trihalide perovskite, *Adv. Energy Mater.* 5 (15) (2015), 1500477.
- [90] H.-S. Kim, J.-Y. Seo, N.-G. Park, Material and device stability in perovskite solar cells, *ChemSusChem* 9 (18) (2016) 2528–2540.
- [91] T. Supasai, et al., Formation of a passivating CH₃NH₃PbI₃/PbI₂ interface during moderate heating of CH₃NH₃PbI₃ layers, *Appl. Phys. Lett.* 103 (18) (2013), 183906.
- [92] B. Philippe, et al., Chemical and electronic structure characterization of lead halide perovskites and stability behavior under different exposures—a photoelectron spectroscopy investigation, *Chem. Mater.* 27 (5) (2015) 1720–1731.
- [93] A. Marques, et al., Low-temperature blade-coated perovskite solar cells, *Ind. Eng. Chem. Res.* 60 (2021).
- [94] Y. Hu, et al., Impact of Rubidium and Cesium cations on the moisture stability of multiple-cation mixed-halide perovskites, *ACS Energy Lett.* 2 (10) (2017) 2212–2218.
- [95] Y. Zhang, et al., Major impediment to highly efficient, stable and low-cost perovskite solar cells, *Metals* 8 (11) (2018).
- [96] T. Baikie, et al., Synthesis and crystal chemistry of the hybrid perovskite (CH₃NH₃)PbI₃ for solid-state sensitised solar cell applications, *J. Mater. Chem. 1* (18) (2013) 5628–5641.
- [97] G. Divitini, et al., In situ observation of heat-induced degradation of perovskite solar cells, *Nat. Energy* 1 (2) (2016), 15012.
- [98] E.M. V, et al., CuI and CuSCN as Hole Transport Materials for Perovskite Solar Cells, 2018.
- [99] K. Leo, Signs of stability, *Nat. Nanotechnol.* 10 (7) (2015) 574–575.
- [100] J. Shi, et al., Hole-conductor-free perovskite organic lead iodide heterojunction thin-film solar cells: high efficiency and junction property, *Appl. Phys. Lett.* 104 (6) (2014), 063901.
- [101] D. Khatiwada, et al., Efficient perovskite solar cells by temperature control in single and mixed halide precursor solutions and films, *J. Phys. Chem. C* 119 (46) (2015) 25747–25753.
- [102] J.S. Shaikh, et al., Nanoarchitectures in dye-sensitized solar cells: metal oxides, oxide perovskites and carbon-based materials, *Nanoscale* 10 (11) (2018) 4987–5034.
- [103] J.A. Christians, P.A. Miranda Herrera, P.V. Kamat, Transformation of the excited state and photovoltaic efficiency of CH₃NH₃PbI₃ perovskite upon controlled exposure to humidified air, *J. Am. Chem. Soc.* 137 (4) (2015) 1530–1538.
- [104] I. Hwang, et al., Enhancing stability of perovskite solar cells to moisture by the facile hydrophobic passivation, *ACS Appl. Mater. Interfaces* 7 (31) (2015) 17330–17336.
- [105] S. Bonabi Naghadeh, et al., Photophysical properties and improved stability of organic-inorganic perovskite by surface passivation, *J. Phys. Chem. C* 122 (28) (2018) 15799–15818.
- [106] I.C. Smith, et al., A layered hybrid perovskite solar-cell absorber with enhanced moisture stability, *Angew. Chem. Int. Ed.* 53 (42) (2014) 11232–11235.
- [107] C. Eames, et al., Ionic transport in hybrid lead iodide perovskite solar cells, *Nat. Commun.* 6 (1) (2015) 7497.
- [108] W. Tress, et al., Understanding the rate-dependent J-V hysteresis, slow time component, and aging in CH₃NH₃PbI₃ perovskite solar cells: the role of a compensated electric field, *Energy Environ. Sci.* 8 (3) (2015) 995–1004.
- [109] J.H. Noh, et al., Chemical management for colorful, efficient, and stable inorganic-organic hybrid nanostructured solar cells, *Nano Lett.* 13 (4) (2013) 1764–1769.
- [110] X. Li, et al., A vacuum flash-assisted solution process for high-efficiency large-area perovskite solar cells, *Science* (2016) 353.
- [111] L. Xu, et al., Minimizing performance degradation induced by interfacial recombination in perovskite solar cells through tailoring of the transport layer electronic properties, *Apl. Mater.* 6 (3) (2018), 036104.
- [112] C. Liu, et al., Efficient and stable perovskite solar cells prepared in ambient air based on surface-modified perovskite layer, *J. Phys. Chem. C* 121 (12) (2017) 6546–6553.
- [113] J. Cao, et al., Efficient grain boundary suture by low-cost tetra-ammonium zinc phthalocyanine for stable perovskite solar cells with expanded photoresponse, *J. Am. Chem. Soc.* 140 (37) (2018) 11577–11580.
- [114] A. Steele Julian, et al., Thermal unequilibrium of strained black CsPbI₃ thin films, *Science* 365 (6454) (2019) 679–684.
- [115] J. Chen, et al., Effect of bidentate and tridentate additives on the photovoltaic performance and stability of perovskite solar cells, *J. Mater. Chem. 7* (9) (2019) 4977–4987.
- [116] G. Grancini, et al., One-Year stable perovskite solar cells by 2D/3D interface engineering, *Nat. Commun.* 8 (1) (2017), 15684.